Optogenetic Manipulation of Covert Attention in the Nonhuman Primate

Leor N. Katz[1], Martin O. Bohlen[2], Gongchen Yu[1], Carlos Mejias-Aponte[1], Marc A. Sommer[2], and Richard J. Krauzlis[1]

Abstract

■ Optogenetics affords new opportunities to interrogate neuronal circuits that control behavior. In primates, the usefulness of optogenetics in studying cognitive functions remains a challenge. The technique has been successfully wielded, but behavioral effects have been demonstrated primarily for sensorimotor processes. Here, we tested whether brief optogenetic suppression of primate superior colliculus can change performance in a covert attention task, in addition to previously reported optogenetic effects on saccadic eye movements. We used an attention task that required the monkey to detect and report a stimulus change at a cued location via joystick release, while ignoring changes at an uncued location. When the cued location was positioned in the response fields of transduced neurons in the superior colliculus, transient light delivery coincident with the stimulus change disrupted the monkey's detection performance, significantly lowering hit rates. When the cued location was elsewhere, hit rates were unaltered, indicating that the effect was spatially specific and not a motor deficit. Hit rates for trials with only one stimulus were also unaltered, indicating that the effect depended on selection among distractors rather than a low-level visual impairment. Psychophysical analysis revealed that optogenetic suppression increased perceptual threshold, but only for locations matching the transduced site. These data show that optogenetic manipulations can cause brief and spatially specific deficits in covert attention, independent of sensorimotor functions. This dissociation of effect, and the temporal precision provided by the technique, demonstrates the utility of optogenetics in interrogating neuronal circuits that mediate cognitive functions in the primate. ■

INTRODUCTION

Since the advent of optogenetics, remarkable advances have been made in dissecting the complex interactions between brain and behavior. The success of optogenetics has been most notably observed in the animal model in which it had been pioneered, the rodent, whereas progress in the nonhuman primate (NHP) has been more limited (Bliss-Moreau, Costa, & Baxter, 2022; Tremblay et al., 2020). This is primarily because of the substantially larger volume of NHP brains, the efficacy with which viral vectors are able to deliver transgenes of interest, and the complexity of the primate immune system and its response to viral vectors (Daw et al., 2023; Bjornson-Hooper et al., 2022). The challenge to successfully apply optogenetic techniques in the NHP is therefore ongoing, and is an important one, because successful application of optogenetics in the NHP will lead to a better understanding of the primate nervous system and, in the longer term, could be leveraged for the treatment of neurological and psychiatric disorders (Daw et al., 2023; Bliss-Moreau et al., 2022; Tremblay et al., 2020; Chow & Boyden, 2013; Deisseroth, 2012).

Prior efforts at using optogenetics in NHPs have demonstrated effects at the anatomical, neurophysiological, and behavioral levels (for reviews, see El-Shamayleh & Horwitz, 2019, and Deng, Yuan, & Dai, 2018). Effects on behavior have been the most challenging and, when achieved, could be because of impairments in sensory processing, motor action, or cognitive functions. Sensory impairments have been observed in experiments in which visual areas were suppressed, causing changes to visual discrimination (e.g., Fetsch et al., 2018; Afraz, Boyden, & DiCarlo, 2015). Motor disruptions have been seen when oculomotor areas were manipulated to alter eye-movement responses (e.g., El-Shamayleh, Kojima, Soetedjo, & Horwitz, 2017; Inoue, Takada, & Matsumoto, 2015). Effects on cognitive function are less straightforward, because behavioral impairments that appear cognitive in nature could also be because of alterations in sensory or motor processes required to complete the task, if such competing interpretations are not ruled out. This ambiguity arises when manipulations are applied to brain areas involved in a particular modality (e.g., an area of the visual system), and the behavioral response is directly linked to that modality (e.g., a saccadic response; Andrei, Pojoga, Janz, & Dragoi, 2019; Nandy, Nassi, Jadi, & Reynolds, 2019; Dai, Brooks, & Sheinberg, 2014). Some studies have

[1]National Eye Institute, [2]Duke University

Journal of Cognitive Neuroscience 37:2, pp. 266–285
https://doi.org/10.1162/jocn_a_02274

effectively addressed this problem by using a different effector (Ghosh & Maunsell, 2024; Hüer, Saxena, & Treue, 2024), but the extent to which optogenetics in the NHP can reliably cause changes in cognitive behavior functions remains a persistent challenge, despite its obvious importance.

Our approach here builds on observations that pharmacologic suppression of neural activity in the midbrain superior colliculus (SC) during a covert visual attention task impairs behavioral performance in a way that cannot be explained by disruptions to sensory or motor processes. Monkeys in these studies reported their answer with a motor response that is not associated with SC function: the manual release of a joystick (Bogadhi, Katz, Bollimunta, Leopold, & Krauzlis, 2021; Herman, Katz, & Krauzlis, 2018; Lovejoy & Krauzlis, 2010). These previous studies used muscimol, an agonist for GABA receptors, to suppress the SC—a useful but relatively nonspecific approach. Unlike optogenetics, pharmacological manipulations last for several hours, involve compensatory mechanisms, and do not provide precise temporal control or the ability to target particular classes of neurons. It has not yet been established whether brief optogenetic suppression at temporally specific epochs would be strong enough to lead to similar results. Here, we used a visual attention task with the goal of determining whether optogenetic suppression of SC could elicit comparable impairments in attention task performance and whether these impairments could be attributed to disruptions of cognitive processes as opposed to sensory or motor functions.

We used a virus with robust expression in primate SC (Cushnie et al., 2020) to deliver the inhibitory opsin Jaws and optimized our approach based on previous reports (Acker, Pino, Boyden, & Desimone, 2016). Behavioral testing began with guided saccade tasks, used primarily as positive controls. We found that 500-msec-long optogenetic suppression in SC, coincident with the go signal of the saccade task, slowed saccadic RTs in both visual and memory-guided versions of the task. Having established the effectiveness of the optogenetic suppression, we then turned to testing for possible effects on the attention task. We found that light delivered for a brief interval coincident with the change in the attended stimulus reduced the monkey's detection performance, even though the monkey maintained fixation throughout the task and reported the answer by releasing a joystick. We show that the impairment was specific to the portion of the visual field affected by the opsin virus injection, was because of an elevated perceptual threshold for detecting events at the affected location, and was present only when there were competing stimuli. These results demonstrate that, in addition to influencing sensory and motor processes, optogenetic approaches in the NHP can be successfully used with high temporal precision to manipulate cognitive functions such as covert visual attention.

METHODS

Animals

One adult male rhesus monkey (*Macaca mulatta*) was used in the study (aged 15 years, weight: ~10 kg). All experimental protocols were approved by the National Eye Institute Animal Care and Use Committee, and all procedures were performed in accordance with the United States Public Health Service policy on the humane care and use of laboratory animals. A plastic headpost and recording chamber had been implanted, 38° posterior to vertical on the sagittal plane (schematized in Figure 1A), and centered on the cranial midline, granting electrophysiological access to both the right and left SC, as described previously (Herman, Arcizet, & Krauzlis, 2020; Arcizet & Krauzlis, 2018).

Experimental Apparatus

The animal was seated and head-fixed in a primate chair (Crist Instrument Inc.) inside a darkened booth facing a 100-Hz VIEWPixx display (VPixx Technologies) that was controlled by a mid-2010 Mac Pro (Apple Inc.) running MATLAB (The MathWorks) with the Psychophysics Toolbox extensions (Brainard, 1997). Experiments were controlled using a modified version of PLDAPS (Eastman & Huk, 2012). Eye position was recorded using an EyeLink 1000 infrared eye-tracking system (SR Research Ltd.) and monitored online for gaze-contingent progression through the task. Manual responses were collected with a single-axis joystick (CH Products, Model HFX-10) mounted out of view to the frontal panel of the primate chair and oriented to allow vertical movement.

Guided-saccade Task

A guided-saccade task (Katz, Yu, Herman, & Krauzlis, 2023; Lovejoy & Krauzlis, 2010) was used to measure the spatial extent of the suppressive effect ("the suppressive field") and to obtain a positive control confirming the saccade-related deficits of SC suppression.

Measuring the "Suppressive Field"

The spatial extent of the suppressive field (Figure 2B) was determined by using a grid of potential target locations tiling the visual field from −15° to 15° on the x axis and from −10° to 10° on the y axis, at a spacing of either 2.5° or 5°, with smaller spacing dedicated to locations matching the expected site of the optogenetic effect. Overall, 81 target locations were used for visually guided saccades, both with and without light delivery at the transduced site, netting 162 unique trial types per block (Target Location × Light Condition). This experimental configuration was used in two experimental sessions with the optrode located in the same location in SC, yielding 2819 successfully completed trials. Results were consistent across the two sessions and were combined to increase statistical power.

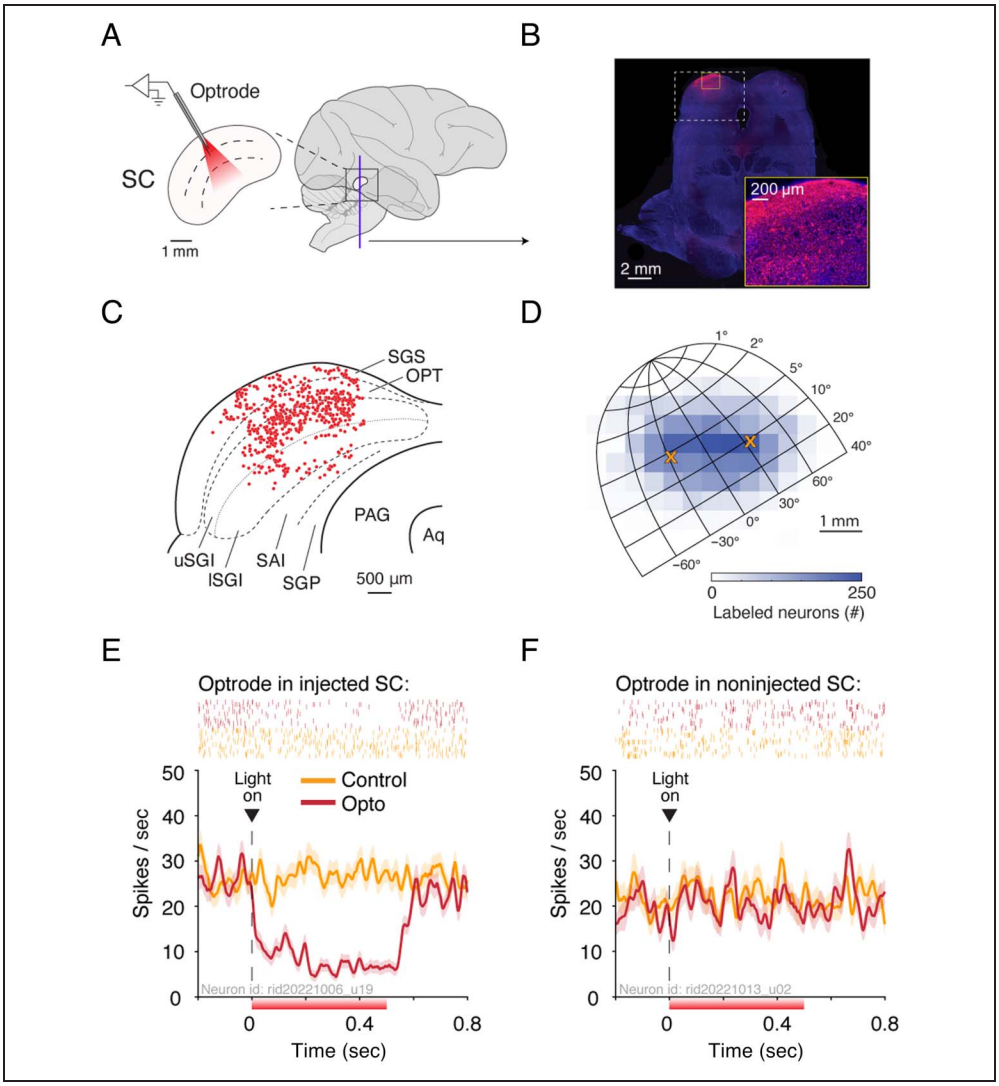

Figure 1. Light delivery to primate SC suppressed neuronal activity. (A) Experimental approach. An optrode was positioned just above the intermediate layers of SC where rAAV2-Retro-CBA-Jaws-KGC-mCherry-WPRE had been delivered by injection. (B) Digital photomicrograph of a representative SC coronal section with cells expressing the fluorescent protein mCherry, confirming successful viral transduction. Magnified version presented in yellow box. Dashed white box indicates the area of SC used for reconstruction in C. (C) A reconstruction of the injected SC highlights the laminar distribution of mCherry-positive somata. (D) The distribution of labeled SC neurons projected onto a topographical map of SC. Orange X symbols indicate the estimated locations of virus injection, based on functional mapping of neuronal receptive fields. (E) Optogenetic suppression of SC neuronal activity. Rasters (top) and PETH (bottom) of an example neuron in the injected SC, aligned to light delivery for the opto conditions and to time-matched moments for the control condition. Neuron ID is indicated above the abscissa. Red bar below the abscissa indicates the duration of light delivery. (F) Absence of optogenetic suppression for an example neuron in the noninjected SC (same format as E). Aq = cerebral aqueduct; lSGI = lower sublamina of the intermediate gray layer; OPT = stratum opticum; PAG = periaqueductal gray; SAI = intermediate white layer; SGP = deep gray layer; SGS = superficial gray layer; uSGI = upper sublamina of the intermediate gray layer.

Positive Control Tasks

Saccade-related deficits were confirmed before each attention task session (described next, below) using the guided-saccade task. For this purpose, potential targets were assigned to predefined locations in the visual field: Saccade targets appeared either contralateral or ipsilateral to the transduced SC (i.e., inside or outside the suppressive field, respectively). In addition, trials were either visually guided or memory guided, and light was either delivered or not. Each trial type had equal probability, netting eight unique trial types in a block. Overall, we collected 27 sessions using this configuration, with 228 ± 26 trials (mean ± *SD*) in each.

In this article, we report results for saccade trials that were either visually guided (Figure 2) or memory-guided (Figure 3). Both types of trials were randomly interleaved within a block and occurred in equal proportion. In all versions of the guided-saccade task trials, a trial was initiated when the monkey pressed down the joystick to trigger the appearance of a 0.25° wide white fixation square (48 cd/m^2) on a gray background (28.5 cd/m^2). Fixation had to be maintained within a 1.5° wide square window (invisible to the monkey). At 0.5–0.7 sec after fixation acquisition, a 0.25° wide square-shaped white saccade target (48 cd/m^2) appeared at some peripheral location (depending on task configuration, detailed below) and either remained visible (visually guided condition) or disappeared after 0.2 sec (memory-guided condition). The monkey was required to maintain fixation during target presentation up until the disappearance of the fixation square (the go signal, 1–2 sec after target onset) and then make a saccade toward the target within 0.1–0.5 sec, land within a 3° wide window around the target (invisible to the monkey), and then maintain fixation within the window for a duration of 0.5–0.7 sec. The precise timings of

events on every trial were determined by random draws from a uniform distribution within the prescribed ranges. In the memory-guided condition, the target reappeared for 0.2 sec after entrance of the eye trace into the target window. Successful completion of a trial resulted in a juice reward. Trials with errors were aborted and then reshuffled into the block of trials.

Covert Attention Task

We used a standard covert attention paradigm (Herman et al., 2020; Arcizet & Krauzlis, 2018) that is schematized in Figure 3A. In this task, the subject is required to respond with the release of a joystick located in the center of the primate chair, while maintaining fixation throughout the trial. Thus, the response is spatially decoupled from the attended location and does not involve oculomotor circuitry.

A trial was initiated when the monkey pressed down the joystick to trigger the appearance of a 0.25° wide white fixation square (48 cd/m^2) on a gray background (28.5 cd/m^2). Fixation had to be maintained within a 1.5° wide square window (invisible to the monkey). Two hundred fifty milliseconds after fixation acquisition, a cue appeared in the form of a ring (inner radius: 3.75°, outer radius: 4°) for a brief duration of 200 msec at an eccentricity of 7–10°, positioned to match the location of the suppressive field (Figure 2B). The location of the spatial cue was constant for a block of 144 trials and then switched to a mirror-opposite location across the vertical meridian. Five hundred milliseconds after the cue ring was extinguished, two circular motion stimuli (3° radius) were presented: One coincided with the location of the cue; the other, in the mirror-opposite location. The visual-motion stimuli consisted of moving dots (48 cd/m^2), with the direction of motion of each dot drawn from a normal distribution with a mean value (defined as motion direction) and a 16° standard deviation. Dot density was 25 dots/deg^2/sec, speed was 15°/sec, and the dot lifetime was set to 100 msec and initiated so that 1/10th of the dots were reborn on each frame. Motion direction was in one of four equally probable directions (toward the fixation point, away, or orthogonal to that axis), determined pseudorandomly on every trial.

Motion stimuli remained on for a duration of 1–3 sec, whereupon a change in motion direction occurred either in the stimulus coincident with the cue location (termed a "cued change") or in the opposite stimulus (termed a "foil change"). On cued-change trials, the monkey received a liquid reward for responding to the change by releasing the joystick within 200–800 msec after the change ("hit" in signal detection terms). On foil-change trials, the monkey received a liquid reward for ignoring the change and maintaining the joystick pressed until the end of motion presentation ("correct reject" in signal detection terms). Failing to respond to a cued change ("miss") or failure to ignore the foil change ("false alarm") resulted in no reward. The ratio of cued changes to foil changes was 3:1. On 12.5% of trials, only one motion stimulus was presented. In these trials, the cue location was always coincident with stimulus location (i.e., a cued change) and occurred at the beginning of a block to remind the monkey of the rule.

Overall, 16 sessions of the covert attention task were collected. In all sessions, the magnitude of the motion-direction change varied from trial to trial, selected pseudorandomly from a range of change magnitude values. In 6 of the 16 sessions, three change-magnitude values were used, typically 15°, 18°, and 21°, where the range was selected to bracket the threshold stimulus difficulty and achieve an average hit rate of ~70%. Magnitude values were sampled with equal probability. In the remaining 10 of 16 sessions, eight change-magnitude values were used and spanned a larger range, 8–30°, to measure psychometric functions. Magnitude values in these "psychometric sessions" were sampled with larger weights on near-threshold magnitude values to better constrain the psychometric function fits. The data presented in Figures 4 and 6 were collected from all 16 sessions but constrained to only include trials with a near-threshold range of magnitude values: 14–24°. Data in Figure 5 were collected during the 10 psychometric sessions and include trials for the full range of magnitude values. To visualize the psychometric function, we pooled data from all 10 sessions (Figure 5A and D), and to quantitatively test for statistical significance, we quantified the function parameters on a session-by-session basis (Figure 5B, C, E, and F). Motion-direction changes in all sessions occurred either clockwise or counterclockwise with equal probability, determined pseudorandomly on every trial. Overall, 1031 ± 200 trials (mean ± *SD*) were collected per session.

Covert Attention Task Sample Size

The sample size of 16 sessions was selected based on an a priori power analysis using G*Power (Faul, Erdfelder, Lang, & Buchner, 2007), where 16 was determined as the number of sessions required to detect medium or higher effect sizes ($dz > 0.6$; Cohen, 1988) with standard alpha and beta settings (alpha = 0.05, beta = 0.7). Post hoc, the effect size produced in the experiment, based on the difference of means between light and no-light conditions (also referred to as "opto" and control conditions), their standard deviations, and correlation between conditions, was $dz = 1.9$, achieving maximal power. Reducing the alpha to a more conservative value of 0.01 netted a power of 0.99. One NHP was sufficient to achieve high statistical power (Fries & Maris, 2022) in addressing our central question: whether or not optogenetic suppression in primate SC is sufficiently efficacious to induce behavioral effects in a selective attention task that does not involve saccades. The use of additional animals could provide further validation, but because our results are consistent with previous, less specific, manipulations using pharmacological

agents in the SC (Bogadhi et al., 2021; Herman et al., 2018; Lovejoy & Krauzlis, 2010), we concluded that using additional animals for this study was not strongly justified.

The number of trials required for inclusion was based on a power analysis for binomial data. Within each attention task session, 42 was determined as the minimum number of trials for a given condition (e.g., cued change, foil change, cued change of single motion stimulus), based on a medium effect size ($g = 0.15$) and standard settings (alpha = 0.05, beta = 0.7). Across the 16 sessions, only one session had insufficient trials in the single motion stimulus condition and was therefore excluded from analysis.

Virus Injection

The viral vector, rAAV2-Retro-CBA-Jaws-mCherry-WPRE 5.0×10^{12} vg/mL (Duke Viral Core), drove expression of the suppressive halorhodopsin protein, Jaws. This virus has exhibited strong expression in primate SC (Cushnie et al., 2020). The virus was pressure injected using a gas-tight Hamilton syringe (1701 SN SYR, 10 μL, cemented NDL, 32G, point style 3, needle length: 100 mm). The syringe was held by an in-house custom-made stepping microdrive that could independently drive the syringe and the plunger.

Virus injections were made along two tracks in the left SC. These tracks mapped onto two locations in visual space, above and below the horizontal meridian ([35°, 11°] and [−30°, 6°], polar angle and eccentricity, respectively), which encompassed the intended stimulus placement in our behavioral tasks. In each track, we selected injection sites that corresponded to the intermediate layers of SC, identified based on neurophysiological observations of a preponderance of visuomotor neurons (Katz et al., 2023). We further confirmed that our sites corresponded to the intermediate SC layers by injecting muscimol (a GABA-A agonist) a week before virus injection and observing saccadic deficits to the expected location in the visual field, consistent with muscimol injection into the intermediate layers of SC (Bogadhi et al., 2021; Lovejoy & Krauzlis, 2010).

When making the virus injections along the first track, we advanced the syringe 0.2 mm deeper than the designated injection site in the intermediate layers and left the cannula to rest at that position for 10 min. We then retracted the cannula by 0.2 mm whereupon 1 μL of virus was infused over a period of 10 min (a 0.008-μL pulse every 5 sec, 125 pulses overall). The cannula was allowed to rest for 5 min after injection to promote diffusion from the needle tip, then retracted 0.5 mm for an injection at a second site (following the same injection protocol), and then retracted another 0.5 mm for an injection at a third site. This process was then repeated at the second SC track during the same experimental session. Overall, 6 μL of virus was injected over six sites across two tracks within the left SC. Data collection began 4 months after the virus injections and lasted 5 months.

Optogenetic Suppression and Extracellular Recording of SC Neurons

We used a 100-mW 635-nm laser (RLM635TA-100FC, Shanghai Optics) coupled to custom-built optrodes. The optrodes consisted of a 75-μm-wide tungsten sharp electrode (UEWLCESE1NNE, FHC) attached to a 200-μm optic fiber (0.37 NA, Doric Lenses Inc.) that was tapered using an electrode puller (P2 puller, Narishige International). The tapered fiber increased the area illuminated by the laser, following the approach detailed in Acker and colleagues (2016). The optic fiber and electrode were glued together with the electrode tip protruding 500 μm from the optic fiber tip. Laser power was measured at the optrode tip (photodiode sensor and Centauri power meter, Ophir Optronics Solutions) and adjusted using a power supply (ADR-180A, Shanghai Optics) to reach 10-mW (250 mW/mm^2). To obtain stable power for optogenetic suppression, the laser was left on throughout the experiment, and a 500-msec period of constant light delivery was controlled by a switch (CO12-M5-FC-1-5H, Luminos) that provided a transition time from the "off" to "on" state of less than 1 msec. The same power level and delivery duration were used on every experimental session.

On every session, the optrode was lowered into SC using a custom-built stepping microdrive, and extracellular signals were amplified, filtered, and digitized at 40 kHz (Omniplex-A, Plexon). The optrode was lowered into one of the two locations in which virus was injected, and the location within SC was verified on each session by mapping the response fields of the recorded neurons (using the guided-saccade task). Neuronal and behavioral effects of optogenetic suppression did not differ between the two locations in SC. Light was delivered either at randomized times while the animal freely viewed a nature documentary on the monitor, or at specific times within the visually guided saccade task, the memory-guided saccade task, or the covert-attention task (see Figures 2A, 3A, and 4A, respectively). The duration of light delivery was 500 msec in all cases. The duration of light delivery was selected based on the allotted window to execute a saccade in the visually guided saccade task used as a positive control. In the task, the monkey was required to execute a saccade within 100–500 msec after the go signal (mentioned above). Using a light duration of 500 msec starting with the go signal guaranteed that the saccades would be generated during the delivery of light, not before or after. This duration is also sufficiently long to include the saccadic burst of SC neurons associated with an eye movement in the guided saccade task (Katz et al., 2023) as well as the response of SC neurons to a stimulus change in the covert attention task (Bogadhi et al., 2021).

Over the course of an experimental session, light was delivered during free viewing, the saccade tasks, and the covert-attention task, and delivered every 12.5 sec on average, with a minimum of 4 sec between consecutive deliveries. The short and infrequent periods of light delivery ensured minimal (if any) tissue heating (Acker et al., 2016), such that effects because of changes in temperature should be negligible. The effect of light delivery on neuronal activity was observed in real time and analyzed offline after spike sorting (Offline Sorter, Plexon). Single units were isolated when possible; otherwise, we considered them multiunit. Other than the well-isolated example neurons presented in Figures 1C–D, 2C, 3B, and 4B, we refer to all other units as "units," as these include both neurons and multiunits.

Immunostaining

After conclusion of the experiments, the animal was sedated with ketamine HCl and then deeply anesthetized with sodium pentobarbital (50 mg/kg, intravenous). Once completely areflexic, the animal was transcardially perfused with 6L of 0.1M, pH 7.2 phosphate-buffered saline (PBS), followed by 4L of 4% paraformaldehyde in 0.1M, pH 7.2 PB. The brain was then divided into three blocks (frontal, thalamic, and visual cortical) in situ in the frontal plane. The brain was then postfixed for approximately 24 hr at 4°C, in the 4% paraformaldehyde solution before being transferred to a 30% sucrose in 0.1M PB (pH 7.2) buffer at 4°C for cryoprotection. Once the blocks had sunk in the sucrose solution, the tissue was frozen and serial sections of the blocks were made in the frontal plane, 75 μm thick, using a freezing stage sliding microtome (American Optical Company). Sections were then stored in PBS at 4°C until they were immunohistochemically processed.

Detailed protocols regarding immunofluorescent amplification of viral labeling were described previously (Daw et al., 2023). Briefly, serial free-floating sections were rinsed in PBS, permeated with triton before being incubated in a triton + BSA blocking solution. Sections were then incubated on a shaker plate in rabbit anti-mCherry (1:200; Rockland, 600-401-P16). Tissue was then rinsed thoroughly with PBS and incubated with donkey antirabbit IgG conjugated with Texas Red (1:200; abcam, ab6800). Free-floating sections were then counterstained by incubating in Hoechst (1:100; Thermo Fisher Scientific, 62249) for 30 min, before being rinsed and mounted on gelatinized subbed glass slides and allowed to dry overnight. Mounted sections were dehydrated through a gradient of ethanol before being moved to toluene. Slides were then coverslipped using Cytoseal 60 (Thermo Fisher Scientific). Bright field digital photomicrographs were acquired using a Zeiss Axio Scan.Z1 affixed with a Hitachi HV F202 color camera (Carl Zeiss Microscopy, LLC). The microscope and cameras were controlled using Zeiss ZEN 2.3 software.

Projection of Labeled Cells onto Topographic Map of SC

Coronal sections with neurons expressing the viral label mCherry (11 sections overall, 450 μm apart) were matched to coronal plates of a standard stereotactic atlas (Paxinos, Huang, Petrides, & Toga, 2008). This resulted in a distribution of labeled neurons in a common reference frame, spanning Plates 80–90 of the atlas. Plates were cropped between 10 and 20 mm dorsoventral and 0 and 8 mm mediolateral in Adobe Illustrator and exported at a resolution of 10 μm per pixel. The exported images were then loaded into imageJ (Schneider, Rasband, & Eliceiri, 2012) where the center point of each labeled cell was segmented and transformed into a single pixel. To account for the 450-μm spacing between each 10 × 8 mm exported image, we inserted 22 blank images before and after each exported image, netting a 3-D volume that matched the physical dimensions of the sectioned volume (i.e., 22 + 1 + 22 images, each 10 μm deep, resulting in 450 μm). The volume was resliced into the sagittal plane, rotated −38° to align the volume with our SC chamber and resliced horizontally, resulting in a top–down view of labeled neurons, in accordance with standard topographical maps of the SC (Chen, Hoffmann, Distler, & Hafed, 2019; Ottes, Van Gisbergen, & Eggermont, 1986; Robinson, 1972). Labeled neurons were summed within 450-μm-wide isotropic voxels and collapsed along the z axis to form a 2-D heatmap. The heatmap was aligned with a recent topographic map of SC (Chen et al., 2019) by aligning the heatmap area of highest cell count to the location of virus injection in SC (Figure 1D).

Behavioral Analysis and Model Fitting

All analyses were performed in MATLAB (The MathWorks). All hypothesis testing between conditions was done using nonparametric tests: Statistical tests on paired samples (e.g., on the matched opto and control conditions) were Wilcoxon signed-rank; tests on unpaired data were Wilcoxon rank-sum.

Attention task behavioral data from psychometric sessions were concatenated and analyzed with a maximum likelihood fit of a two-parameter logistic function (Katz, Yates, Pillow, & Huk, 2016; Wichmann & Hill, 2001) assuming a Bernoulli distribution of binary choices, in which the probability of a joystick release is P and no release is $1 - P$, where P is given by

$$P = \frac{1}{1 + e^{-\beta(x-\alpha)}}$$

where x is the magnitude of motion direction change (z scored over all sessions), α is the threshold parameter (reflecting the midpoint of the function in units of change magnitude), and β is the slope (i.e., sensitivity, in units of log odds per change magnitude). Error estimates on the parameters were obtained from the diagonal of the

inverse Hessian (second derivative matrix) of the negative log-likelihood. To evaluate whether parameter values differed significantly between conditions, we used the samples of parameter estimates from individual psychometric sessions, corrected for multiple comparisons.

To test whether effect magnitude changed over time (Figure 5A and B), we fit models to data from each condition (control and opto), where the predictor variable was the number of days since injection. A linear model was used for the normally distributed RT data of the guided saccade task (MATLAB's fitlm); a generalized linear model was used for the binomially distributed data of the covert attention task (MATLAB's fitglm). Overlap between the slope parameter estimates ± standard errors indicated no significant change over time, whereas no overlap indicated the opposite.

Neuronal Analysis

Spike times were aligned to task events and used to construct peri-event time histograms (PETHs) for summaries of firing rates versus time. For the rasters presented in Figure 1, spike times were binned into 1-msec nonoverlapping bins. For the PETHs presented in Figures 1, 2, and 3, spike times were binned into 5-msec nonoverlapping bins and smoothed with a Gaussian kernel with a standard deviation of 5 msec for visualization purposes. Spike counts in prescribed windows (Figures 2D and 3C) were performed with no smoothing.

RESULTS

We used the inhibitory, red-shifted halorhodopsin Jaws to test the effects of suppressing neuronal activity in macaque SC on behavior in a covert attention task. Testing was performed in a well-trained monkey that had reached stable performance in the behavioral tasks. Experimental sessions consisted of two sessions to map the affected region of the visual field (the "suppressive field") and 27 sessions to determine the effect of SC suppression on behaviors directed toward the suppressive field. Saccade-related deficits were confirmed in all 27 sessions, and the effects of SC suppression on covert attention were tested in 16 of the 27 sessions in a manual response task that did not involve saccades. The key advance of our study is the demonstration that optogenetic suppression of the primate SC, delivered at precise moments in the covert attention task for a mere 500 msec, has effects on this cognitive function that are comparable in size to that found in previous studies using coarser pharmacological manipulations.

Light Delivery to Primate SC Suppressed Neuronal Activity

Before evaluating the effect of light delivery to SC on behavior, we first confirmed that light delivery suppressed neuronal activity. We positioned an optrode just above the intermediate layers of SC to maximize light delivery to sites at which the virus was injected (Figure 1A). Histology performed at the conclusion of the experiments confirmed that expression of the opsin was strong at the injection sites and surrounding tissue (Figure 1B). We found no reduction in nuclear labeling around the sites of transduction, indicating that the viral transduction and subsequent light delivery did not cause cellular atrophy or toxicity in the SC. A reconstruction of the histological slice showed the distribution of labeled cells and confirmed that expression was centered on the intermediate layers of SC, with some spread into the overlying superficial layers (Figure 1C). The distribution of labeled cells across 11 histological slices was quantified in a 3-D volume and projected onto a 2-D topographic map of SC (see Methods), showing the spatial extent of viral transduction in the colliculus (Figure 1D).

When light was delivered to the injected SC during free viewing, we observed robust suppression of neuronal activity (example neuron in Figure 1E). The cessation of activity lasted for the full duration of light delivery (0.5 sec). Activity then resumed to baseline levels, demonstrating the temporally specific nature of the optogenetic manipulation. No changes in activity were observed in time-matched control trials, when no light was delivered. When light was delivered to the noninjected SC on the opposite hemisphere, where no expression was expected (Bohlen et al., 2020), no light-driven modulation was observed of neurons in that SC (example neuron in Figure 1F). Quantification of the optogenetically suppressed firing rates across our sample of neurons is described in the next sections. These effects at the single-neuron level demonstrated that viral transduction and expression of the opsin were restricted to the injected SC (consistent with (Bohlen et al., 2020) and that suppression was not because of the mere delivery of light or its corollaries (e.g., heat).

Optogenetic Suppression Induced Strong Behavioral Effects in Saccade Tasks

Optogenetic suppression in SC was previously shown to affect visuomotor behavior in a classic visually guided saccade task (Cavanaugh et al., 2012). We therefore adopted a similar saccade task as a positive control for our optogenetic manipulation. In the visually guided saccade task, the monkey was required to fixate a central point while a peripheral target appeared. Once the central point disappeared (the go signal), the monkey made a saccade to the target to obtain a reward (Figure 2A). On the basis of previous results (Cavanaugh et al., 2012), light delivery coincident with the go signal was expected to delay the initiation of saccades toward the target when it appeared in locations consistent with the response fields of the

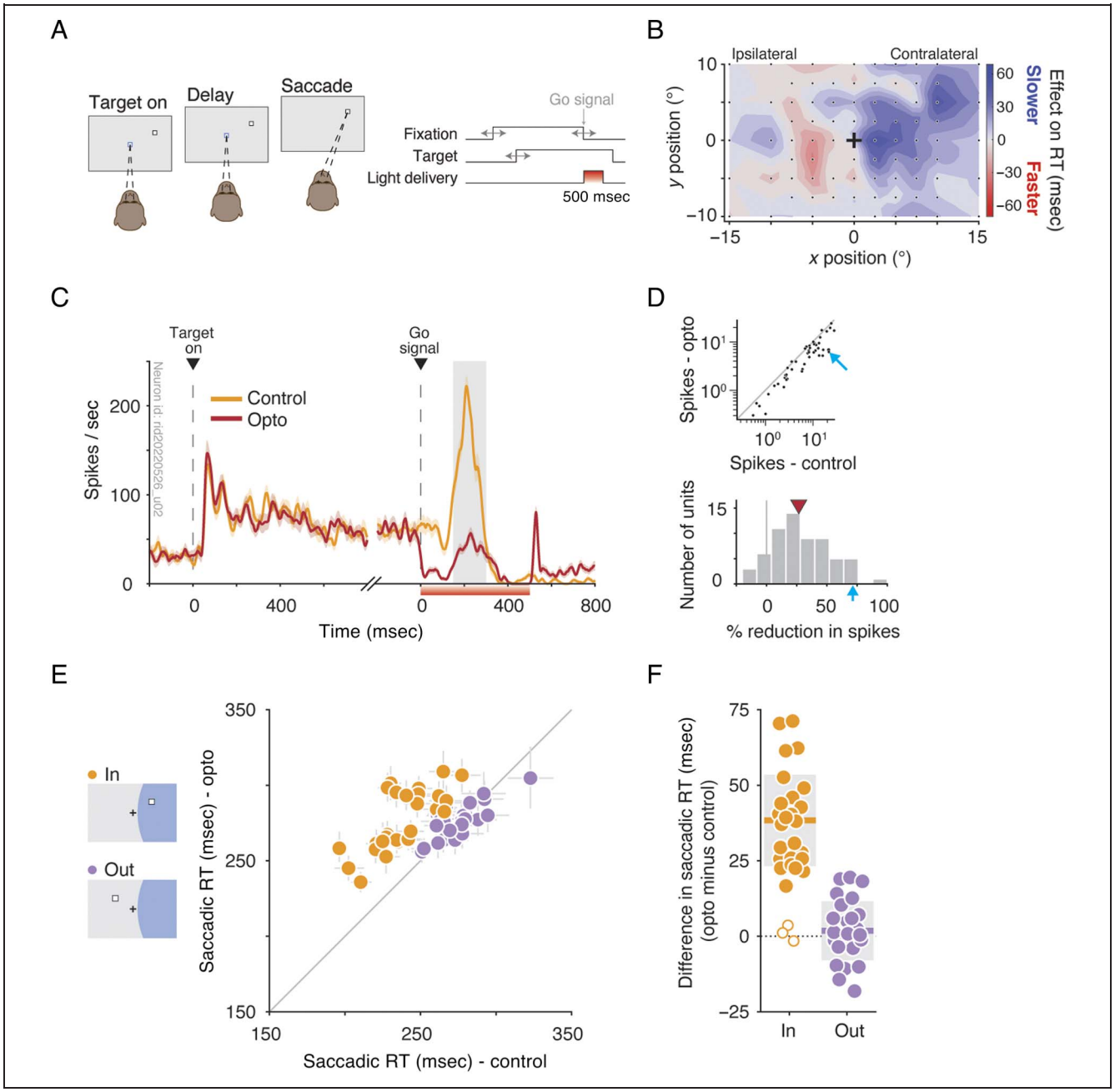

Figure 2. Optogenetic suppression in SC induces behavioral effects in the visually guided saccade task. (A) A visually guided saccade task was used as a positive control. Key events in the task are depicted (left), and their sequence is indicated (right). Double-headed arrows indicate random variability in timing. Light delivery started with the offset of the fixation spot (i.e., the go signal). (B) The effect of light delivery to SC on saccadic RTs to 81 targets that tiled the visual field, averaged over two experimental sessions. Black dots denote target positions, and the black crosshair denotes the fixation point. Color bar indicates the difference in saccadic RTs on trials with light delivery versus trials without. Targets on the left were ipsilateral to the manipulated SC; targets on the right were contralateral. (C) PETH of an example neuron during the visually guided saccade task, aligned to target onset and the go signal. Neuron ID is indicated near the ordinate. Red bar below the abscissa indicates the period of light delivery. Gray rectangle indicates the window in which optogenetic suppression magnitude was computed for D. (D, top) Mean number of spikes within the window indicated in C (150–300 msec after light delivery) for the control and opto conditions, for all units recorded in the task (log scale). Gray line indicates line of unity. Cyan arrow indicates the example neuron in C. (Bottom) Percent reduction in spikes for the same units. Red triangle indicates the median. Cyan arrow on the abscissa indicates the percent reduction for the example neuron in C. (E) Saccadic RTs for the opto and control conditions, for trials in which the target appeared either in or out of the suppressive field (indicated by schematics on the left). Each dot is a session mean. Error bars are 95% confidence intervals. (F) The difference in saccadic RTs between the opto and control conditions summarized for when the target was either in or out of the suppressive field. Each dot shows data from one session; colored bar and gray rectangle indicate the mean ± standard deviation across sessions. Three smaller dots in white show data from three control sessions in which the optrode was placed in the noninjected SC.

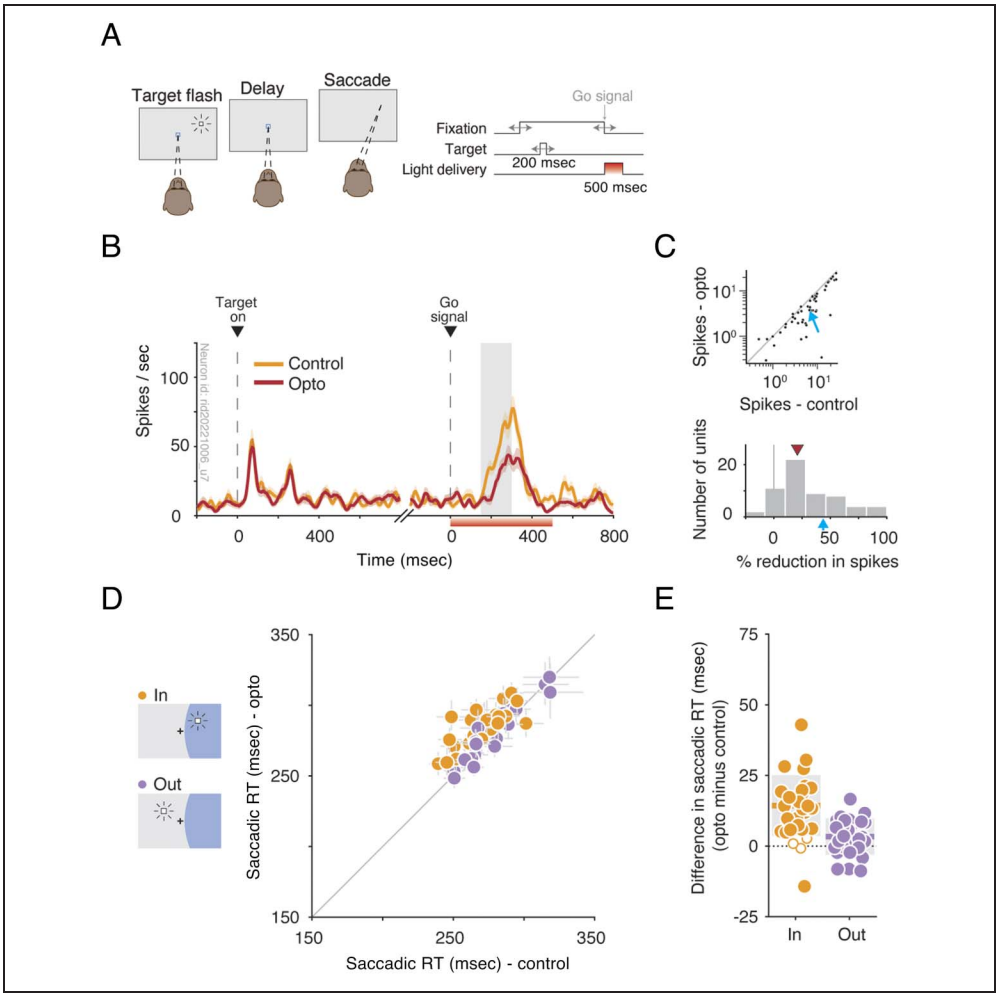

Figure 3. Optogenetic suppression in SC induces behavioral effects in a memory-guided saccade task. (A) Key events in the memory-guided saccade task (left) and their temporal sequence (right). Double-headed arrows indicate random variability in timing. The onset of light delivery was aligned to fixation offset (i.e., the go signal). (B) PETH of an example neuron during the memory-guided saccade task, aligned to target onset and the go signal. Neuron ID is indicated near the ordinate. Red bar below the abscissa indicates the duration of light delivery. Gray rectangle indicates the window in which optogenetic suppression magnitude was computed for B. (C, top) Mean number of spikes within the window indicated in C (150–300 msec after light delivery) for the control and opto conditions, for all units recorded in the task (log scale). Gray line indicates line of unity. Cyan arrow indicates the example neuron in B. (Bottom) Percent reduction in spikes for the same units. Red triangle indicates the median. Cyan arrow on the abscissa indicates the percent reduction for the example neuron in B. (D) Saccadic RTs for the opto and control conditions, for trials in which the target flashed either in or out of the suppressive field (indicated by schematics on the left). Each dot is a session mean. Error bars are 95% confidence intervals. (E) The difference in saccadic RTs between the opto and control conditions summarized for when the target flashed either in or out the suppressive field. Each dot is a session; colored bar and gray rectangle reflect the mean ± standard deviation across sessions. Three white dots show data from three control sessions in which the optrode was placed in the noninjected SC.

transduced neurons, leading to an increase in saccadic RTs for those locations.

We found that optogenetic suppression led to unexpectedly large increases in saccadic RTs. The study of Cavanaugh and colleagues reported a saccadic RT increase of ~7 msec to targets placed in the center of transduced neurons' response field. In contrast, we observed increases that were almost an order of magnitude larger, ~60 msec for targets appearing in the center of the affected region of the visual field (Figure 2B), comparable to the effects of pharmacological inactivation using muscimol (Bogadhi, Bollimunta, Leopold, & Krauzlis, 2019; Bollimunta, Bogadhi, & Krauzlis, 2018). The effect of optogenetic suppression on saccadic RTs was highest for locations in the hemifield contralateral to the suppressed SC and consistent with the sites of virus injections, based on response field measurements taken before virus injection.

Saccades to targets located in the hemifield ipsilateral to the suppressed SC were not as affected and, in some locations, exhibited a slight decrease in RTs. By measuring saccadic RTs to target locations that tiled visual space over two experimental sessions, with versus without optogenetic suppression, we estimated the spatial extent of the optogenetic effect on saccadic RTs, which we term the "suppressive field." The suppressive field was consistent with the projection of transduced neurons onto a topographic map of SC (Figure 1D). The distribution of neurons was centered on eccentricities of approximately 2–20° and on angles of elevation of ±60°, which is consistent with the contours of the suppressive field measured in the saccade tasks. This indicates that the spatial extent of the effects on saccadic RTs was limited by the volume of transduced neurons in the tissue, not by our choice of light delivery methods such as fiber diameter and light intensity.

An example SC neuron recorded during trials in which the target was placed inside its response field, and inside the overlapping suppressive field, exhibited typical responses for a visual-movement SC neuron during the control condition: a strong visual response after the onset of the target and a saccadic burst of spikes that accompanied the saccade shortly after the go signal (Figure 2C; Katz et al., 2023). During the opto condition, spiking was dramatically muted immediately after light delivery. The saccadic burst was still observed, but it was substantially reduced in magnitude. Over the population of units recorded during these trials ($n = 48$), a significant reduction in spikes was observed during the saccadic burst ($p < 1e{-}9$), leading to a mean reduction of 27% across units ($p < 1e{-}10$; Figure 2D). After light cessation, a short-lived rebound may be observed in the example neuron. Rebound activity was observed in approximately half of the neurons recorded but is unlikely to have affected behavior (Acker et al., 2016) and did not vary systematically with suppression magnitude ($p = .6$, Pearson correlation).

We documented the effects of the optogenetic suppression on visually guided saccades to the center of the suppressive field ("in" condition; Figure 2E). Across 27 experimental sessions, suppression increased saccadic RTs from 238 ± 20 msec (control trials, mean ± *SD*) to 276 ± 20 msec (optogenetic suppression trials, $p < 1e{-}5$, Wilcoxon signed-rank), an almost 40-msec increase in saccadic RTs overall (Figure 2F). The increases were consistent across sessions and significant on all 27 individual sessions ($p < .05$ for each, Wilcoxon rank-sum test). Saccades to a target placed outside the suppressive field ("out" condition) were not affected ($p = .32$). Other saccadic metrics such as peak velocity and saccadic endpoint error of saccades to targets placed in the suppressive field were also affected by optogenetic suppression, albeit less consistently: Peak velocity was reduced from 752 ± 129°/sec to 648 ± 157°/sec ($p < 1e{-}3$), and endpoint error increased from 0.9 ± 0.2° to 1.2 ± 0.3° ($p < 1e{-}3$).

In addition to visually guided saccades, we also tested for effects on randomly interleaved memory-guided saccades. The sequence of events in this version of the task was identical to that in the visually guided version, except that the saccadic target did not remain visible for the entirety of the trial. Instead, the target flashed for a duration of 200 msec, and the monkey was required to saccade toward its remembered location after the go signal (Figure 3A). An example SC neuron recorded during memory-guided saccade trials illustrates the typical activity pattern for a visual-movement SC neuron: a brisk onset response to the target flashing in its response field, an offset response 200 msec later, and burst of spikes at the time of the saccade toward the remembered location of the target (Figure 3B; Katz et al., 2023). During the opto condition, spiking was reduced during the saccadic burst. Across the population of units recorded in memory-guided saccade trials ($n = 48$), we observed a significant reduction in spikes during the saccadic burst ($p < 1e{-}10$), with a mean reduction of 21% ($p < 1e{-}8$; Figure 3C).

In the memory-guided version of the saccade task, optogenetic effects on saccadic RTs were observed to a lesser extent (Figure 3D). Optogenetic suppression during memory-guided saccade trials increased saccadic RTs by about 15 msec (Figure 3E), from 268 ± 16 msec (control trials, mean ± *SD*) to 283 ± 14 msec (optogenetic suppression trials, $p < 1e{-}4$, Wilcoxon signed-rank). This delay in generating memory-guided saccades was smaller than that observed in visually guided saccades and was also not as consistent: It was statistically significant in 13 of 27 sessions ($p < .05$ for each, Wilcoxon rank-sum test), as opposed to the 26 of 27 for visually guided saccades. Peak velocity of memory-guided saccades toward the target placed in the suppressive field was reduced from 509 ± 89°/sec to 462 ± 78°/sec ($p < 1e{-}4$), and saccadic endpoint scatter increased from 1.8 ± 0.4° to 2.1 ± 0.3° ($p < 1e{-}4$).

In summary, optogenetic suppression in SC during visually guided saccades increased RTs by almost 40 msec, providing a strong positive control for the effectiveness of the optogenetic manipulation. Optogenetic suppression also delayed memory-guided saccades, but to a lesser extent (~15 msec). For both saccade types, the difference in results between "in" and "out" target position conditions was significant ($p < 1e{-}5$ for visually guided, $p < 1e{-}4$ for memory guided; Wilcoxon signed-rank), demonstrating the spatial specificity of the optogenetic suppression. Finally, light delivery to the nontransduced SC, performed on three sessions and expected to have no behavioral effect (indicated on Figures 2F and 3D in inverted colors), indeed had no significant effect on saccadic RTs to either target, for either type of saccade (statistical tests on all sessions considered jointly or severally, all ps > .05), indicating that the effects on saccadic RTs were specific to the localized viral expression of the light-sensitive opsin and cannot be explained by extraneous factors (e.g., tissue heating).

Optogenetic Suppression Impaired Performance in a Covert-attention Task That Does Not Involve Saccades

We tested the efficacy of optogenetic suppression in SC on behavior in a covert-attention task (Figure 3A; Methods section). In the task, a spatial cue appeared in either the left or right hemifield, followed by the appearance of two motion patches, one in each hemifield. One of the two motion patches was positioned inside the suppressive field, and light was delivered for 500 msec starting at the time of the motion-direction change. On each of the 18 attention task sessions, we first confirmed that suppression led to a statistically significant effect in the positive control saccade task (Figure 2). Once confirmed, we

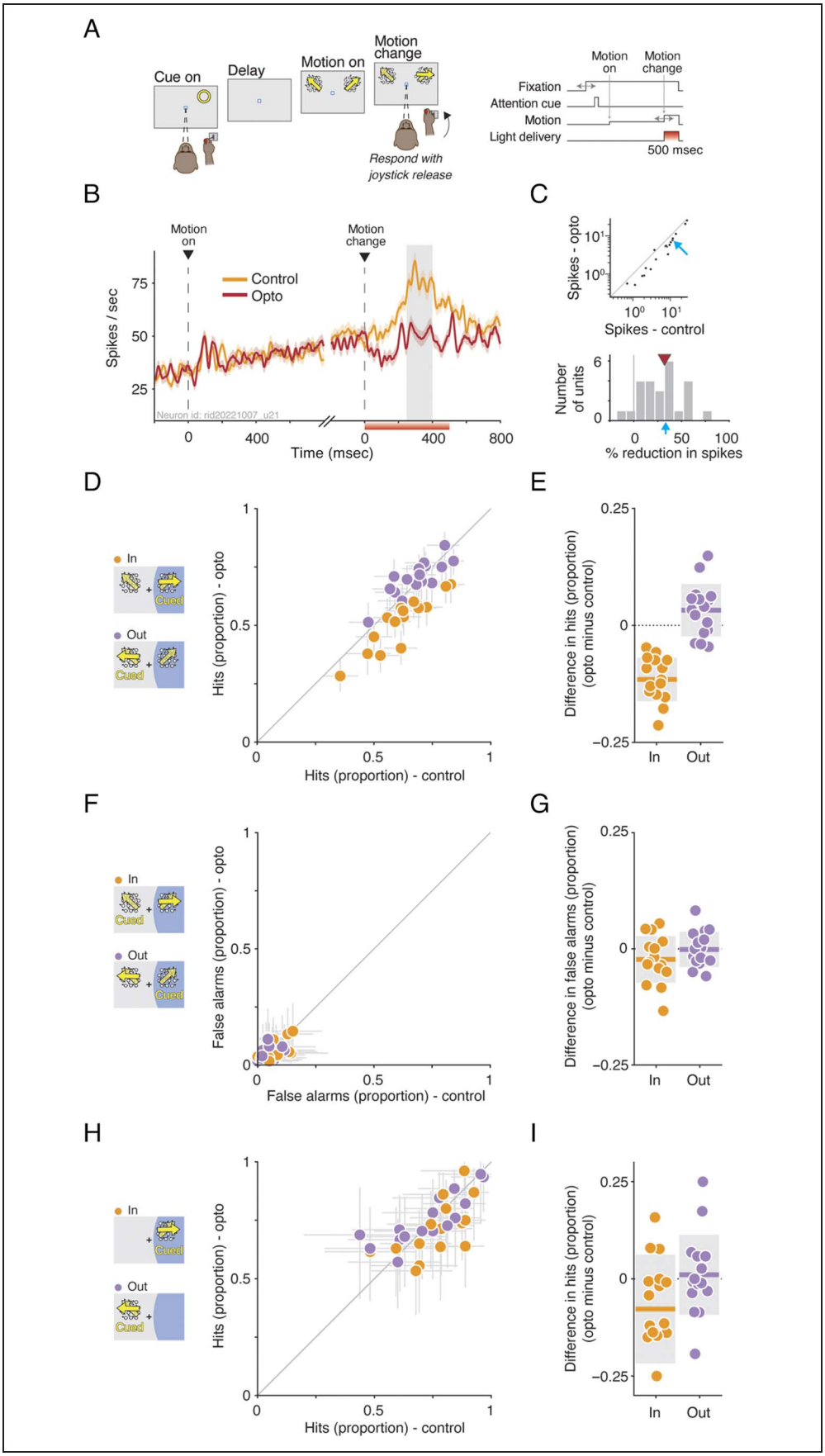

Figure 4. Optogenetic suppression in SC induces behavioral effects in a covert attention task that does not involve saccades. (A) The covert attention task. Key events in the task are depicted (left), and their sequence is indicated (right). Double-headed arrows indicate random variability in timing. The onset of the light delivery coincided with the motion change. (B) PETH of an example neuron during the covert attention task, aligned to motion onset and the time of motion change. Neuron ID is indicated above the abscissa. Red bar below the abscissa indicates the duration of light delivery. Gray window indicates the window in which optogenetic suppression magnitude was calculated for C. (C, top) Mean number of spikes within the window indicated in B (250–400 msec after light delivery) for the control and opto conditions, for all units recorded in the task (log scale). Gray line indicates line of unity. Cyan arrow indicates the example unit in B. (Bottom) Percent reduction in spikes for the same units. Red triangle indicates the median. Cyan arrow on the abscissa indicates the percent reduction for the example neuron in B. (D) Proportion hits (i.e., joystick releases to motion changes that occurred on the same side as the preceding cue) for the opto and control conditions, for trials in which the cued motion change occurred either in or out the suppressive field (indicated by schematics on the left). Each dot is a session mean. Error bars are 95% confidence intervals. (E) Summary of the differences in proportion hits between the opto and control conditions when the motion change was either in or out the suppressive field. Each dot is a session; colored bar and gray rectangle reflect the mean ± standard deviation across sessions. (F–G) Similar format to D–E, but for the proportion of false alarms (i.e., joystick releases to motion changes that occurred on the opposite side to the preceding cue). (H–I) Similar format to D–E, but for the proportion of hits when only a single patch of motion was present.

proceeded to test for effects of optogenetic suppression in the covert-attention task. To ensure that deficits in making saccades would not confound behavioral responses in the attention task, we required the monkey to report its responses manually with a joystick while maintaining central fixation.

An example SC neuron demonstrates the effect of optogenetic suppression in the attention task, when the cued-motion patch was presented at a location matching both the neuron's response field and the optogenetic suppressive field (Figure 4B). In the control condition, shortly after motion stimulus onset, there was an abrupt increase in activity, followed by a gradual increase in activity during the delay period, consistent with previous reports (Bogadhi et al., 2021; Herman et al., 2018). Shortly after the motion-direction change, a second phasic increase in activity was evident; this change-related activity has been causally linked to performance in similar covert-attention tasks (Herman et al., 2018). In the opto condition, this second phasic increase in activity was still present but was substantially reduced because of the optogenetic suppression. Over the population of units recorded in this task ($n = 25$), spike counts during the second phasic increase in activity (indicated with a gray window in Figure 4B) were significantly reduced ($p < 1e{-}4$), leading to an overall 31% reduction in neuronal activity after the motion-direction change ($p < 1e{-}4$; Figure 4C).

Behavioral performance in the task was impaired by transient optogenetic suppression of SC at the time of stimulus change (Figure 4D). For cued-stimulus changes that occurred inside the suppressive field (the "in" condition), light delivery at the time of stimulus change reduced the mean hit rate from 63% in control trials to 52% in the interleaved optogenetic trials ($p < 5e{-}4$, Wilcoxon signed-rank). The reduction in hit rate was observed in almost every session and was statistically significant for six individual sessions out of 16 ($p < .05$, chi-square test for proportions). For cued-stimulus changes that occurred outside the suppressive field ("out"), no reduction was observed ($p = .16$), and the magnitude of effects for the "in" versus "out" conditions differed significantly (Figure 4E, $p < 1e{-}4$), indicating that the impairment was spatially specific. For stimulus changes that occurred opposite to the side of the cue (i.e., "foil changes"), the proportion of joystick releases (i.e., false alarms) was unchanged by light delivery that coincided with a foil change in the suppressive field ($p = .26$) or out ($p = .55$; Figure 4F and G). Thus, optogenetic suppression in SC impaired the monkey's ability to detect a cued stimulus change, and the impairment was spatially specific.

We attribute the impairment during the covert-attention task to disruption of cognitive processing, because possible explanations based on local sensory processing, motor disruptions, or other factors cannot explain the results. First, the reduction in hit rate could not be due to a motor impairment because cued changes could occur either in or out of the suppressive field, whereas the manual response, a joystick release, was identical across cue conditions. If optogenetic suppression had influenced the motor system, it would have impaired performance in both cue conditions. Second, the reduction in hit rate could not be because of disruptions of arousal or motivation because these functions are also not spatially specific. It also cannot be attributed to the type of compensation observed after pharmacological inactivation (Wilke, Kagan, & Andersen, 2012) because optogenetic suppression trials were interleaved with control trials at random and light was delivered only transiently. Third, the impairment cannot be explained as a local deficit in visual processing. Previous studies using pharmacological inactivation in SC reported that deficits were related to selective attention, and not by an impairment to early visual processing, because they required the presence of competing visual stimuli (Lovejoy & Krauzlis, 2010). We found a similar result here. On a subset of trials in the attention task, we presented only a single motion patch. Because no distractor stimulus was present on these "single-patch" trials, the monkey was not required to select the cued stimulus over the uncued, and an impairment in these trials would indicate a deficit in local visual processing. We found no difference in the proportion of hits between the opto and control conditions for this single-patch condition, for changes in or out of the suppressive field ($p = .06$ and $p = .75$, respectively; Figure 4H and I). Moreover, there was a significant difference between the behavioral effect magnitude in the single-patch condition and the double-patch condition ($p < 1e{-}3$, Wilcoxon rank-sum test), where effect magnitude was measured as the percent reduction in hit rate between opto and control conditions. Thus, the effect of optogenetic suppression in SC on selective attention is consistent with an impairment in cognitive processing that cannot be explained by impairments in motor control or to disruptions to local sensory processing.

The Effect of Optogenetic Suppression in the Covert-attention Task Was Consistent with a Change in Threshold

The performance deficits in the covert-attention task could stem from several factors, including a shift in psychophysical threshold (also referred to as a bias), lower psychophysical sensitivity, or some combination of the two. To clarify which aspects of behavior are impaired during SC suppression, we repeated the attention experiment, including several different stimulus change magnitudes, and then modeled task performance using standard psychometric functions.

Performance in these 10 "psychometric sessions" and its disruption due to suppression in SC was similar to that observed in the standard version of the task: Hit

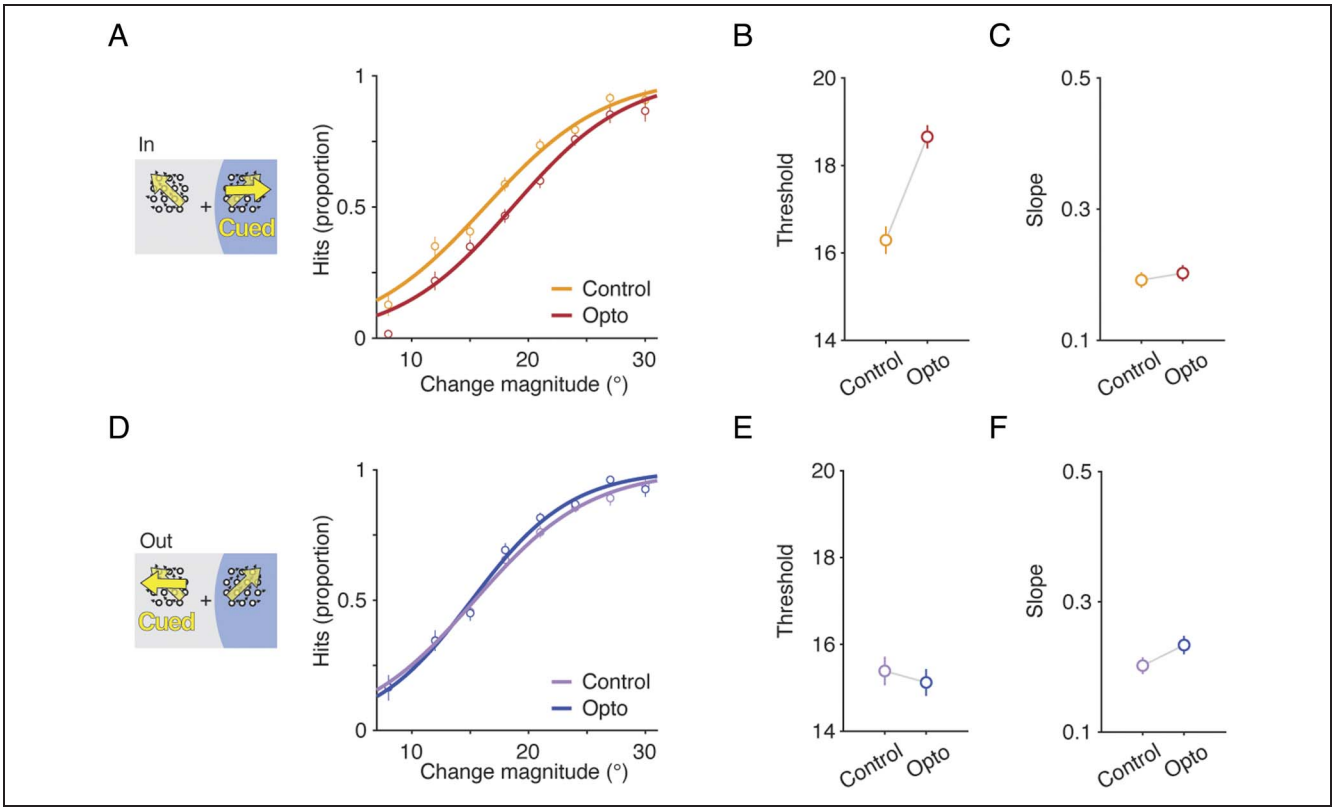

Figure 5. The effect of optogenetic suppression in the covert-attention task is consistent with a change in threshold. (A) Proportion hits (i.e., joystick releases to motion changes that occurred on the same side as the preceding cue) for the opto and control conditions, for trials in which the cued-motion change occurred in the suppressive field (indicated by schematics on the left). Each dot is the mean across trials from all psychometric sessions, concatenated. Error bars are 95% confidence intervals. Thick lines indicate the psychometric functions fit to trial data. (B) Mean value of the psychometric function's threshold parameter for the opto and control conditions, over 10 sessions (error bars are 1 *SEM*). (C) Similar format to D, but for the slope parameter. (D–F) Similar format to A–C, but for trials in which the cued-motion change occurred out of the suppressive field.

rates for cued changes in the suppressive field were lower on trials in which SC was suppressed. This was true for all change magnitudes used (Figure 5A), consistent with a change in psychophysical threshold. Psychometric fits to data from individual sessions allowed us to further quantify this point. These showed that the mean threshold value across sessions, typically defined as the stimulus change magnitude needed to reach a hit rate of 50%, increased from 16.2° for the control trials to 18.7° for trials in which SC was suppressed (Figure 5B; $p < .02$, Wilcoxon signed-rank test). The slope parameter, thought to reflect psychophysical sensitivity, was not significantly changed (Figure 5C; $p = .83$).

For trials in which the cued change occurred outside the suppressive field, hit rates were largely similar across the range of change magnitudes used (Figure 5D), and no statistically significant effect was found on either psychophysical threshold or sensitivity (Figure 5E and F; $p = .28$ and $p = .07$, respectively). In summary, modeling psychometric performance revealed that the behavioral impairment due to SC suppression at the time of stimulus change was best explained as an increase in psychophysical threshold to stimulus changes in the suppressive field.

Reliability of the Optogenetic Effects over Time

The effects of optogenetic suppression persisted for several months in both the saccade tasks and the covert-attention task (Figure 6). In the visually guided saccade task, we found that SC suppression induced an increase of almost 40 msec on average in saccadic RTs to targets positioned in the suppressive field. Such an increase was observed on almost every session (Figure 6A)—even 9 months after the vector injection date—and did not diminish over time (no significant difference between model fit parameters between control and opto conditions; see Methods for evaluation of effect sizes over time).

A similar effect was observed in the memory-guided saccade task, albeit to a lesser extent. The average increase in saccadic RT to targets flashed in the suppressive field was on the order of 15 msec, and it did not diminish significantly over time (Figure 6B).

In the covert-attention task, SC suppression caused a decrease in the proportion of hits for stimulus changes that occurred in the suppressive field. This transiently inducible impairment persisted throughout the duration of testing in this task as well as 9 months after injection and did not decrease significantly over time (Figure 6A).

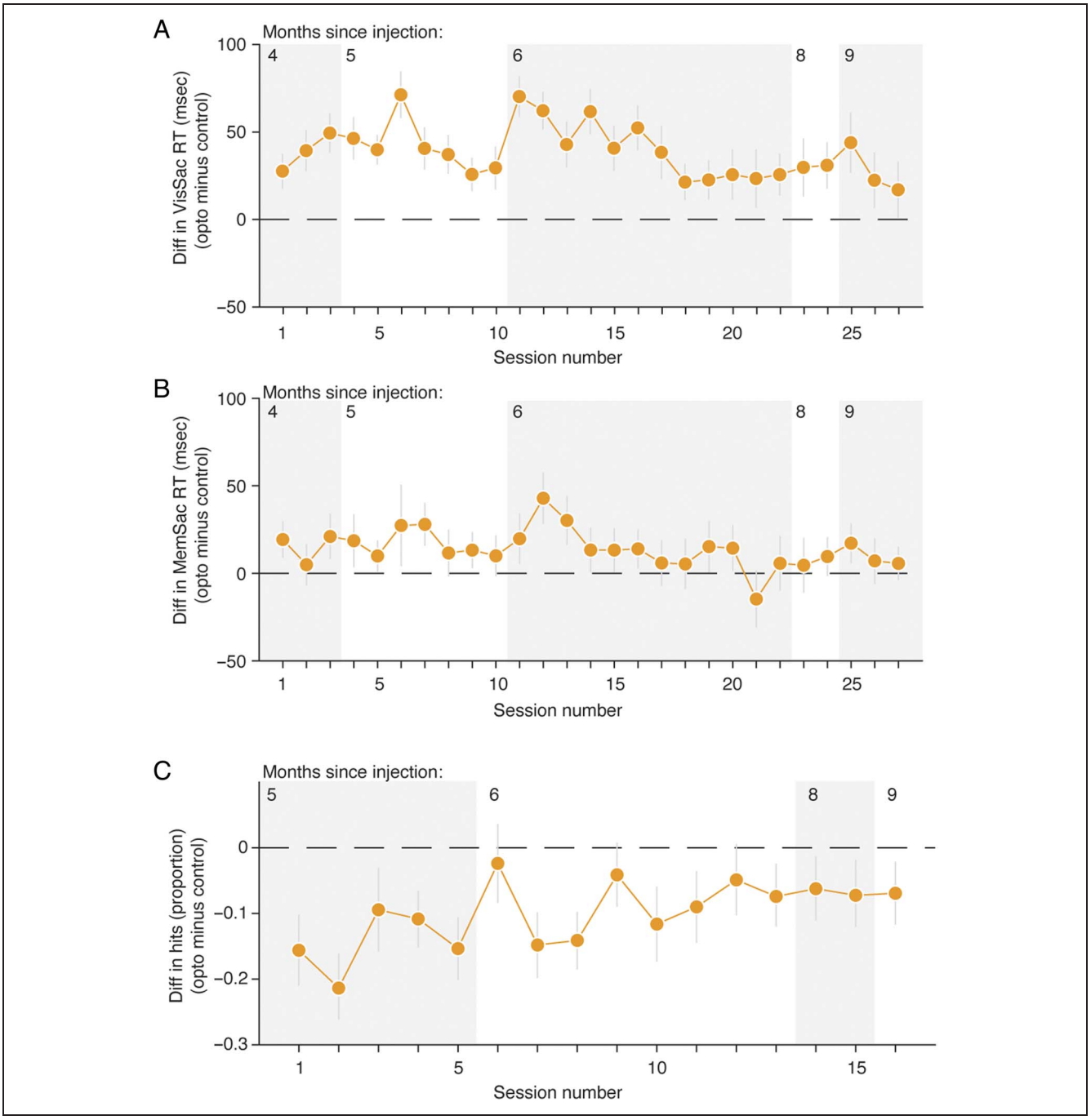

Figure 6. Reliability of the optogenetic effects over time. (A) The behavioral effect of optogenetic suppression in the visually guided saccade task (abbreviated "VisSac"), quantified as the difference in saccadic RTs between the opto and control conditions, over time. Only data to targets placed in the suppressive field are shown. Session number is indicated on the abscissa, and the number of months since injection is indicated on the top of the panel. Error bars are 95% confidence intervals. (B) Similar format to A, but for the memory-guided saccade task (abbreviated "MemSac"). (C) Similar format to A, but for the covert-attention task. Here, the behavioral effect was quantified as the difference in the proportion of hits between the opto and control conditions. Only data for cued-stimulus changes in the suppressive field are shown.

Effects on Behavior Were Uncorrelated across Saccade and Attention Tasks

The effects of optogenetic suppression on the different behavioral tasks were typically measured in the same experimental session and with the optrode located in the same position throughout. This allowed us to assess whether the magnitude of the behavioral effect induced by optogenetic suppression in one task covaried with the magnitude in another. Toward this end, we performed pairwise correlations between effect magnitudes in our three tasks (visually guided saccades, memory-guided saccades, and the covert-attention task).

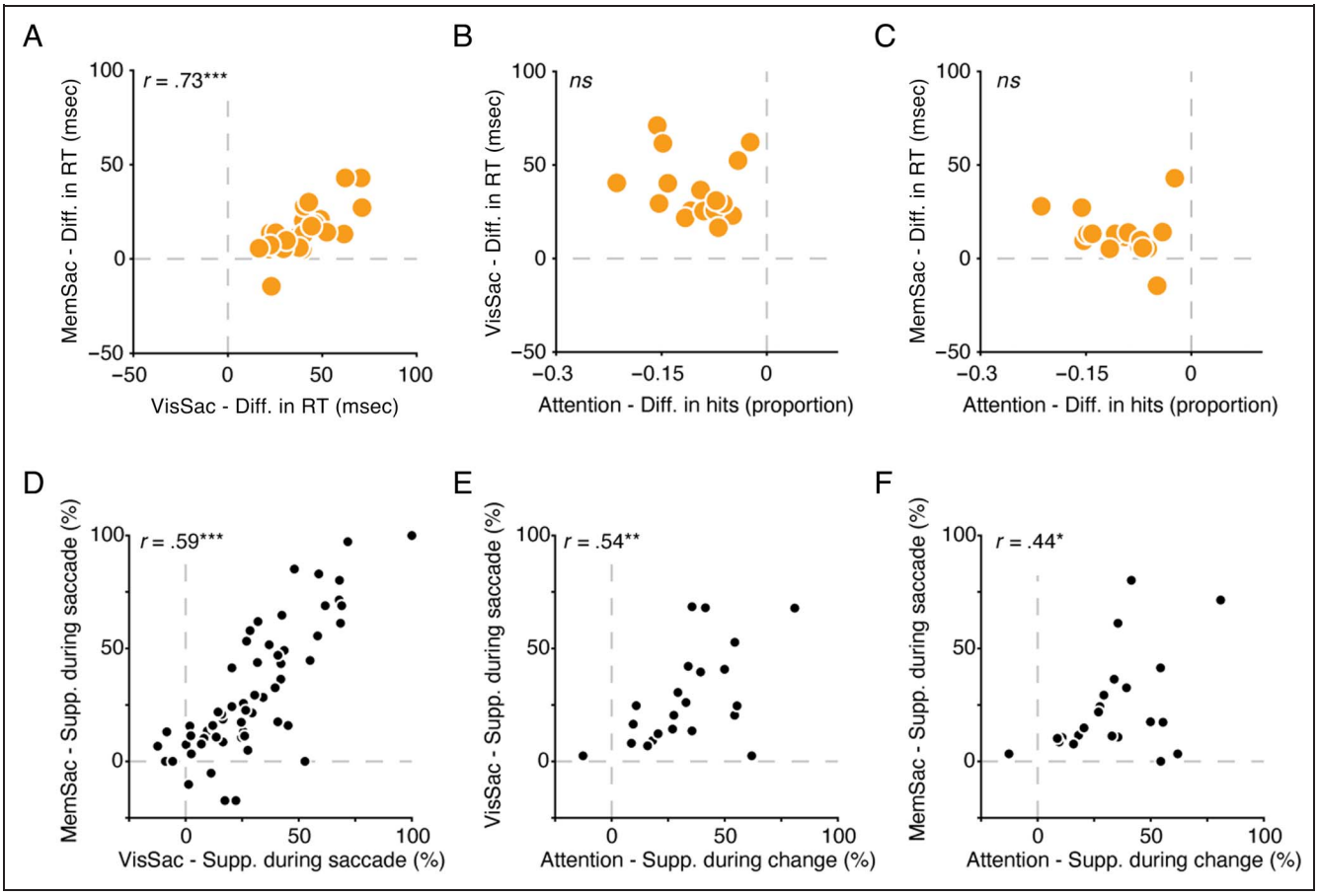

Figure 7. Effects on behavior were uncorrelated across saccade and attention tasks. (A) The difference in saccadic RTs between the opto and control conditions (abbreviated "Diff. in RT") for visually guided saccades ("VisSac) plotted against the difference in RT for memory-guided saccades ("MemSac"). (B–C) Same format as in A, but for the behavioral effect in the covert attention task (difference in the proportion of hits between the opto and control conditions) against difference in RT for visually guided (B) and memory-guided (C) saccades. (D) The magnitude of neuronal suppression during the saccadic burst of the saccade tasks (abbreviated "Supp. during saccade") of visually guided against memory-guided saccades. (E–F) Same format as in D, but for the magnitude of neuronal suppression during the stimulus change of the attention task ("Supp. during change"), against suppression during visually guided (E) and memory-guided (F) saccades.

For the saccade tasks, the effects on RT were evaluated on 27 sessions. We found that the differences in saccadic RTs to targets in the suppressive field between the opto and control conditions (abbreviated "Diff. in RT", Figure 7) were correlated significantly between the visually guided and memory-guided saccade tasks (Pearson $r = .73, p < 1e{-}4$; Figure 7A).

To evaluate the correlation between behavioral effects in the saccade tasks and the attention task, we used the 16 sessions of the covert attention task, which also included the saccade tasks as controls. Despite having run the pairs of tasks in close succession within a session, we found no statistically significant correlation between the differences in RTs for the visually guided saccade task and the differences in hit rate of the attention task ($r = -.18, p = .5$; Figure 7B). Similarly, the differences in RT for the memory-guided saccade task also did not correlate with the difference in hit rate of the attention task ($r = .21$, $p = .4$; Figure 7C).

Next, we performed pairwise correlations between the magnitude of optogenetic effect on neuronal responses. Unlike the magnitude of behavioral effects across tasks, the magnitude of neuronal effect induced by optogenetic suppression correlated in all pairwise permutations of the tasks. The suppression of spikes (in percent) during saccadic bursts (abbreviated "Supp. during saccade") in visually guided trials correlated with the suppression during the memory-guided trials ($r = .59, p < 1e{-}6$; Figure 7D). The suppression of neuronal activity during the stimulus change in the attention task ("Supp. during change") correlated with the suppression during the visually guided saccade task ($r = .54, p < .01$; Figure 7E) and the memory-guided saccade task ($r = .44, p < .05$; Figure 7F).

Thus, optogenetic suppression in SC induced behavioral effects in all tasks over the course of the several months—an increase in saccadic RTs in the visually guided and memory-guided saccade tasks as well as a decrease in the proportion of hits in the attention task. Despite correlated effects on neurons in all three tasks, the variation in behavioral effects correlated only between the two versions of the saccade task and appeared independent of the behavioral effects in the attention task.

DISCUSSION

Optogenetics provides a valuable tool for studying the organization of neuronal circuits and for testing how these circuits control behavior. The technique has been used in the NHP to affect behavior, but its successes have been limited and primarily observed through influencing sensory and motor functions (El-Shamayleh & Horwitz, 2019; Deng et al., 2018). Here, by applying optogenetic approaches in the SC during a covert-attention task, we demonstrate that brief and well-timed optogenetic manipulations can influence cognitive processing in primates, in addition to—but dissociable from—effects on sensorimotor functions.

This conclusion was based on four main results. First, we found that light delivery to the injected SC suppressed the activity of neurons and elicited strong and consistent behavioral effects in paradigms that served as positive controls: visually guided and memory-guided saccade tasks. For visually guided saccades, optogenetic suppression increased saccadic RTs by ~40 msec for targets positioned in the suppressive field (Figure 2). For memory-guided saccades, suppression increased saccadic RTs by ~15 msec (Figure 3). Second, we found that, in a covert-attention task that did not involve saccades, light delivery coincident with the time of the task-relevant event (i.e., the cued-stimulus change) reduced the monkey's ability to detect the event when it occurred in the suppressive field (Figure 4). We showed that the impairment was not because of disruptions of motor control or of deficits in local visual processing but instead seemed specific to a disruption in cognitive functioning related to selective attention. Third, psychometric analysis revealed that the deficit in selective attention could be characterized as an increase in psychophysical threshold (Figure 5). Finally, we found that the effect of optogenetic suppression in the SC on performance in all tasks—the two saccade tasks and the covert-attention task—persisted for 9 months after injection (Figure 6). Thus, our results show that briefly applied optogenetic manipulations in the NHP can induce robust changes in behavior selectively associated with a cognitive process and that these effects can be exerted stably over many months.

Behavioral Effects

One of our main findings is that the behavioral effects of our brief optogenetic manipulation were comparable to those achieved previously using pharmacologic agents. Although the impairment we observed was not a complete inability to register relevant events in the affected visual field, the effect magnitude was sizable, consistent, and replicable over months of testing. Specifically, it was on par with effect sizes observed with pharmacological inactivation of the primate SC (Bogadhi et al., 2021; Herman et al., 2018; Lovejoy & Krauzlis, 2010). The comparability of effect sizes between pharmacology and optogenetics is not trivial given that the light was applied for only a 500-msec interval during the task, whereas microinjections of muscimol exert their inhibitory effects over a large volume of tissue for several hours. Indeed, previous comparisons found optogenetics to be weaker (Afraz et al., 2015). We speculate that the relatively large effects observed here benefited from using tapered fibers and red light to illuminate larger volumes of neural tissue (Deng et al., 2018; Acker et al., 2016), as well as selecting a viral vector shown to express strongly in primate SC (Cushnie et al., 2020). Together, these steps may have contributed to the relatively large behavioral deficits observed in covert attention.

Several aspects of our experimental design allowed us to determine whether the behavioral impairment was because of deficits in sensory, motor, or cognitive function. First, we only observed a reduction in detecting the cued-stimulus change (i.e., hits) when a change occurred in the suppressive field, contralateral to the manipulated SC (Figure 4D and E). Such spatial specificity rules out competing explanations that are not spatially specific such as a motor deficit (because the manual response was a nondirectional joystick release) or changes in arousal and/or motivational systems. Second, we found that when only one patch of motion was presented, no deficit was observed (Figure 4H and I). This rules out deficits in local early visual processing, consistent with findings from pharmacological inactivation of SC during covert-attention tasks (Lovejoy & Krauzlis, 2010). Third, the temporal specificity afforded by the technique allowed us to deliver light at the exact moment the motion stimulus changed, which was the key event to track (Wang, McAlonan, Goldstein, Gerfen, & Krauzlis, 2020; Herman et al., 2018). Taken together, our results indicate that the impairment in the covert-attention task was because of a disruption of mechanisms used for selectively attending a relevant location at the specific moment a stimulus changed and not because of disruptions of local sensory processing or motor control.

We also found that optogenetic suppression impaired behavior in the saccade task used as positive control. This was not surprising: After all, the visually guided saccade task was selected precisely because we expected to see a behavioral effect. The effect magnitude, however, was unexpected. The pioneering study that used optogenetic suppression in SC during a visually guided saccade task (Cavanaugh et al., 2012) reported a modest and inconsistent increase in saccadic latencies, on the order of ~7 msec. A study that used optogenetic suppression in the FEFs reported similarly modest effects (Acker et al., 2016). The effect reported in the current study was ~40 msec on average and, in some sessions, reached ~70 msec, an order of magnitude larger than that reported previously. Furthermore, it was impressively consistent, exhibiting statistical significance in all but one session. Similarly to behavioral effects in the covert attention task, effects in the visually guided saccade task were on par with those observed with pharmacological

inactivation of SC (Bollimunta et al., 2018), demonstrating the efficacy of the approach taken here.

The delay in saccadic RTs caused by optogenetic suppression was larger for visually guided saccades (~40 msec) than for memory-guided saccades (~15 msec). The smaller impact of SC suppression in the memory-guided version of the task is consistent with previous observations using pharmacological inactivation of SC (Hikosaka & Wurtz, 1985). The difference is potentially explained by the contributions of the FEF and lateral intraparietal cortex to saccade motor control; on the basis of pharmacological manipulations, these cortical eye fields play a larger causal role in supporting memory-guided saccades than visually guided saccades (Dias & Segraves, 1999; Li, Mazzoni, & Andersen, 1999).

The behavioral effect induced by optogenetic suppression of SC lasted for several months in all three tasks: visually guided saccades, memory-guided saccades, and the covert attention task (Figure 6). The magnitudes of these effects were highly correlated between the two saccade tasks (Figure 7A), but no correlation was found between the increases in saccadic RTs and the decrease of hit rates in the attention task (Figure 7B and C). The degree of induced neuronal suppression, in contrast, was highly correlated for all pairwise comparisons of the tasks (Figure 7D and F). This indicates that the light-driven hyperpolarization of neurons is not task dependent, whereas the behavioral effects are task dependent, presumably because the functional contributions of these neurons differ across tasks.

The circuitry of the SC supports this idea. The oculomotor role of primate SC has long been emphasized, but a slew of experiments over the past two decades—including the current study—have demonstrated the contributions of SC neurons to higher-order functions and cognitive processing (Basso & May, 2017; Krauzlis, Lovejoy, & Zénon, 2013). These functions may be supported by inputs and outputs that are distinct from those used for sensory and motor function (Katz et al., 2023; Basso & May, 2017; Krauzlis et al., 2013). The lack of correlation found between behavioral effects in the covert attention and guided saccade tasks (Figure 7C) further implies separability of function, subserved by different neuronal circuits within and through the SC.

Optogenetic versus Pharmacological Approaches

Most of the effects reported here, using optogenetic suppression in SC, are in line with those reported in studies using pharmacological inactivation in SC. One study using muscimol in SC, however, found a correlation between the effect magnitudes in a visually guided saccade task and an attention task (Bollimunta et al., 2018), unlike the findings made here (Figure 7B and C). It is tempting to attribute the difference in results to the different volumes of neural tissue affected by optogenetics compared to pharmacology (Afraz et al., 2015), but in fact, the estimated volume affected by high-powered red light emanating from a tapered fiber (Acker et al., 2016) is comparable to that affected by <1 μL of muscimol injection (Arikan et al., 2002; Martin, 1991). Instead, we think this difference points to a potentially important functional difference between the two types of causal manipulations. With muscimol injections, which hyperpolarize neurons somewhat indiscriminately, the variability in outcomes is likely because of differences in the effectiveness of the injections across sessions, producing correlated effects across tasks even if the tasks involve different circuits. In contrast, optogenetic manipulation, because it relies on the long-term viral transduction of cells within the neuronal population, has the potential to be more constant. Our data support this idea, because the variability of optogenetically induced effects across sessions, in both the visually guided saccade task and the covert attention task, was substantially smaller than that observed in a study using muscimol (Bollimunta et al., 2018). In optogenetic studies, it is likely that nearly the same neurons are suppressed across sessions. However, as noted above, those neurons might not be equally involved in the different tasks, leading to independent behavioral effects across tasks.

Unlike muscimol, which hyperpolarizes cell bodies at the site of injection, rAAV2-retro transduces cells both locally and retrogradely (Cushnie et al., 2020). The hyperpolarizing effect of the opsin, therefore, stands to operate both at the soma and at the terminals of neurons projecting to the SC from other brain areas. Both of these targets may have contributed to the behavioral effects observed. However, although light-driven somatic suppression was clearly observed in SC neurons (Figures 2D, 3C, 4C, and 7D–F), it is yet unclear whether photosensitization at the terminals is sufficient to suppress the action potentials coursing down the axon. Moreover, the behavioral results reported here are consistent with those reported in previous studies using muscimol in SC (where only cell bodies are hyperpolarized, because muscimol does not affect fibers of passage), in visually guided saccades, memory-guided saccades, and the covert attention task (Bogadhi et al., 2021; Bollimunta et al., 2018; Hikosaka & Wurtz, 1985). Thus, although it is potentially possible that our manipulation suppressed inputs to SC, the primary effect on behavior is likely mediated through the suppression of cell bodies within the SC, consistent with the strong somatic transduction observed (Figure 1B–D). In either case, the behavioral effects we observed would be due to suppression of signals processed locally within the SC. Further applications of differentially selective viral vectors in the behaving NHP will be needed to examine how both behavioral and neuronal effects depend on transduction of the soma versus projection terminals, and possibly targeting different subpopulations of neurons, potentially providing a powerful new approach for doing detailed functional circuit analysis in NHPs. Indeed, clarifying these circuit-specific properties of viral vectors will be crucial for realizing the translational potential of optogenetics.

Neurophysiological Effects

In optogenetic studies, observing anatomical expression of an opsin is necessary but not sufficient to obtain neurophysiological responses to light, and those, in turn, are necessary but not sufficient to produce an effect on behavior. It follows, then, that effects on behavior must be accompanied by light-mediated effects on neurophysiology and that these must be due to anatomical transduction. The behavioral results we found were accompanied by both opsin expression (Figure 1B–D) and neurophysiological responses (Figures 2D, 3C, and 7). We found that most of the neurons we recorded from reduced their activity in response to light, even with no screening procedures to find and test only light-responsive neurons. Rather, our only criterion was to place the optrode according to the lamination of the SC: It was always positioned just above the intermediate layers, as assessed by standard functional criteria (see Methods section). Overall, the mean reduction in neuronal activity because of optogenetic suppression at key events in the trial—either during the saccadic burst in the saccade tasks or during the change-related response in the covert-attention task—was on par with previous reports of optogenetic suppression in SC using a different opsin (Cavanaugh et al., 2012). The similarity in suppression magnitude is at odds with the larger behavioral effect produced here. We speculate that the larger effects reported here are because of a larger transduction volume, as well as the larger volume illuminated by red light, although this has not been quantitatively measured. It may also be because of the nature of the retrovirus construct, which transduces both cell bodies and axon terminals, leading to suppression of local SC circuitry as well as inputs to the SC.

Conclusions

The ability to influence neuronal activity using optogenetics, at unprecedented spatial and temporal precision, allows researchers to manipulate circuits at high granularity. In the current study, we adopted a simple strategy with the primary intention of producing behavioral effects that are large, interpretable, and replicable, in a task that involves cognitive processing related to selective attention. Even in the absence of targeting specific pathways and cell types—an approach that will surely provide deeper insights into constituent circuit elements, once it becomes available in the NHP—we demonstrated the efficacy of the approach in influencing cognitive processes related to selective attention in the primate, independent of sensory and motor functions. Such a demonstration opens new opportunities to study higher-order functions in the NHP that in the future could lead to treatments of neurological disorders and psychiatric disease in humans (Deng et al., 2018; Chow & Boyden, 2013; Deisseroth, 2012).

Acknowledgments

We thank Nick Nichols, Daniel Yochelson, Denise Parker, and Hayden Warnock for technical support and Genevieve Kuczewski for assistance in histological preparation of the material. We are grateful to Christian Quaia, Adam Messinger, Kara Cover, and Divya Subramanian for helpful discussions.

Corresponding author: Leor N. Katz, Laboratory of Sensorimotor Research, National Eye Institute, Bethesda, MD 20892, e-mail: leor.katz@nih.gov.

Data Availability Statement

Data will be made available upon request by email to the corresponding author.

Author Contributions

Leor N. Katz: Conceptualization; Data curation; Formal analysis; Investigation; Methodology; Project administration; Validation; Visualization; Writing—Original draft; Writing—Review & editing. Martin O. Bohlen: Formal analysis; Funding acquisition; Methodology; Resources; Writing—Review & editing. Gongchen Yu: Investigation; Methodology; Writing—Review & editing. Carlos Mejias-Aponte: Methodology; Resources; Writing—Review & editing. Marc A. Sommer: Funding acquisition; Supervision; Writing—Review & editing. Richard J. Krauzlis: Conceptualization; Funding acquisition; Investigation; Project administration; Resources; Supervision; Writing—Review & editing.

Funding Information

This work was supported by the National Institutes of Health through the National Eye Institute Intramural Research Program (ZIA EY000511) and the National Institute of Neurological Disorders and Stroke external award number R01NS125843. The content is solely the responsibility of the authors and does not necessarily represent the official views of the National Institutes of Health.

Diversity in Citation Practices

Retrospective analysis of the citations in every article published in this journal from 2010 to 2021 reveals a persistent pattern of gender imbalance: Although the proportions of authorship teams (categorized by estimated gender identification of first author/last author) publishing in the *Journal of Cognitive Neuroscience* (*JoCN*) during this period were M(an)/M = .407, W(oman)/M = .32, M/W = .115, and W/W = .159, the comparable proportions for the articles that these authorship teams cited were M/M = .549, W/M = .257, M/W = .109, and W/W = .085 (Postle and Fulvio, *JoCN*, 34:1, pp. 1–3). Consequently, *JoCN* encourages all authors to consider gender balance explicitly when selecting which articles to cite and gives them the opportunity to report their article's gender citation balance.

REFERENCES

Acker, L., Pino, E. N., Boyden, E. S., & Desimone, R. (2016). FEF inactivation with improved optogenetic methods. *Proceedings of the National Academy of Sciences, U.S.A.*, *113*, E7297–E7306. https://doi.org/10.1073/pnas.1610784113, PubMed: 27807140

Afraz, A., Boyden, E. S., & DiCarlo, J. J. (2015). Optogenetic and pharmacological suppression of spatial clusters of face neurons reveal their causal role in face gender discrimination. *Proceedings of the National Academy of Sciences, U.S.A.*, *112*, 6730–6735. https://doi.org/10.1073/pnas.1423328112, PubMed: 25953336

Andrei, A. R., Pojoga, S., Janz, R., & Dragoi, V. (2019). Integration of cortical population signals for visual perception. *Nature Communications*, *10*, 3832. https://doi.org/10.1038/s41467-019-11736-2, PubMed: 31444323

Arcizet, F., & Krauzlis, R. J. (2018). Covert spatial selection in primate basal ganglia. *PLoS Biology*, *16*, e2005930. https://doi.org/10.1371/journal.pbio.2005930, PubMed: 30365496

Arikan, R., Blake, N. M. J., Erinjeri, J. P., Woolsey, T. A., Giraud, L., & Highstein, S. M. (2002). A method to measure the effective spread of focally injected muscimol into the central nervous system with electrophysiology and light microscopy. *Journal of Neuroscience Methods*, *118*, 51–57. https://doi.org/10.1016/S0165-0270(02)00143-7, PubMed: 12191757

Basso, M. A., & May, P. J. (2017). Circuits for action and cognition: A view from the superior colliculus. *Annual Review of Vision Science*, *3*, 197–226. https://doi.org/10.1146/annurev-vision-102016-061234, PubMed: 28617660

Bjornson-Hooper, Z. B., Fragiadakis, G. K., Spitzer, M. H., Chen, H., Madhireddy, D., Hu, K., et al. (2022). A comprehensive atlas of immunological differences between humans, mice, and non-human primates. *Frontiers in Immunology*, *13*, 867015. https://doi.org/10.3389/fimmu.2022.867015, PubMed: 35359965

Bliss-Moreau, E., Costa, V. D., & Baxter, M. G. (2022). A pragmatic reevaluation of the efficacy of nonhuman primate optogenetics for psychiatry. *Oxford Open Neuroscience*, *1*, kvac006. https://doi.org/10.1093/oons/kvac006, PubMed: 38596709

Bogadhi, A. R., Bollimunta, A., Leopold, D. A., & Krauzlis, R. J. (2019). Spatial attention deficits are causally linked to an area in macaque temporal cortex. *Current Biology*, *29*, 726–736. https://doi.org/10.1016/j.cub.2019.01.028, PubMed: 30773369

Bogadhi, A. R., Katz, L. N., Bollimunta, A., Leopold, D. A., & Krauzlis, R. J. (2021). Midbrain activity shapes high-level visual properties in the primate temporal cortex. *Neuron*, *109*, 690–699. https://doi.org/10.1016/j.neuron.2020.11.023, PubMed: 33338395

Bohlen, M. O., McCown, T. J., Powell, S. K., El-Nahal, H. G., Daw, T., Basso, M. A., et al. (2020). Adeno-associated virus capsid-promoter interactions in the brain translate from rat to the nonhuman primate. *Human Gene Therapy*, *31*, 1155–1168. https://doi.org/10.1089/hum.2020.196, PubMed: 32940068

Bollimunta, A., Bogadhi, A. R., & Krauzlis, R. J. (2018). Comparing frontal eye field and superior colliculus contributions to covert spatial attention. *Nature Communications*, *9*, 3553. https://doi.org/10.1038/s41467-018-06042-2, PubMed: 30177726

Brainard, D. H. (1997). The Psychophysics Toolbox. *Spatial Vision*, *10*, 433–436. https://doi.org/10.1163/156856897X00357, PubMed: 9176952

Cavanaugh, J., Monosov, I. E., McAlonan, K., Berman, R., Smith, M. K., Cao, V., et al. (2012). Optogenetic inactivation modifies monkey visuomotor behavior. *Neuron*, *76*, 901–907. https://doi.org/10.1016/j.neuron.2012.10.016, PubMed: 23217739

Chen, C.-Y., Hoffmann, K.-P., Distler, C., & Hafed, Z. M. (2019). The foveal visual representation of the primate superior colliculus. *Current Biology*, *29*, 2109–2119. https://doi.org/10.1016/j.cub.2019.05.040, PubMed: 31257138

Chow, B. Y., & Boyden, E. S. (2013). Optogenetics and translational medicine. *Science Translational Medicine*, *5*, 177ps5. https://doi.org/10.1126/scitranslmed.3003101, PubMed: 23515075

Cohen, J. (1988). *Statistical power analysis for the behavioral sciences* (2nd ed.). Routledge. https://doi.org/10.4324/9780203771587

Cushnie, A. K., El-Nahal, H. G., Bohlen, M. O., May, P. J., Basso, M. A., Grimaldi, P., et al. (2020). Using rAAV2-retro in rhesus macaques: Promise and caveats for circuit manipulation. *Journal of Neuroscience Methods*, *345*, 108859. https://doi.org/10.1016/j.jneumeth.2020.108859, PubMed: 32668316

Dai, J., Brooks, D. I., & Sheinberg, D. L. (2014). Optogenetic and electrical microstimulation systematically bias visuospatial choice in primates. *Current Biology*, *24*, 63–69. https://doi.org/10.1016/j.cub.2013.11.011, PubMed: 24332543

Daw, T. B., El-Nahal, H. G., Basso, M. A., Jun, E. J., Bautista, A. R., Samulski, R. J., et al. (2023). Direct comparison of epifluorescence and immunostaining for assessing viral mediated gene expression in the primate brain. *Human Gene Therapy*, *34*, 228–246. https://doi.org/10.1089/hum.2022.194, PubMed: 36719771

Deisseroth, K. (2012). Optogenetics and psychiatry: Applications, challenges, and opportunities. *Biological Psychiatry*, *71*, 1030–1032. https://doi.org/10.1016/j.biopsych.2011.12.021, PubMed: 22503111

Deng, C., Yuan, H., & Dai, J. (2018). Behavioral manipulation by optogenetics in the nonhuman primate. *Neuroscientist*, *24*, 526–539. https://doi.org/10.1177/1073858417728459, PubMed: 28874078

Dias, E. C., & Segraves, M. A. (1999). Muscimol-induced inactivation of monkey frontal eye field: Effects on visually and memory-guided saccades. *Journal of Neurophysiology*, *81*, 2191–2214. https://doi.org/10.1152/jn.1999.81.5.2191, PubMed: 10322059

Eastman, K. M., & Huk, A. C. (2012). PLDAPS: A hardware architecture and software toolbox for neurophysiology requiring complex visual stimuli and online behavioral control. *Frontiers in Neuroinformatics*, *6*, 1. https://doi.org/10.3389/fninf.2012.00001, PubMed: 22319490

El-Shamayleh, Y., & Horwitz, G. D. (2019). Primate optogenetics: Progress and prognosis. *Proceedings of the National Academy of Sciences, U.S.A.*, *116*, 26195–26203. https://doi.org/10.1073/pnas.1902284116, PubMed: 31871196

El-Shamayleh, Y., Kojima, Y., Soetedjo, R., & Horwitz, G. D. (2017). Selective optogenetic control of purkinje cells in monkey cerebellum. *Neuron*, *95*, 51–62. https://doi.org/10.1016/j.neuron.2017.06.002, PubMed: 28648497

Faul, F., Erdfelder, E., Lang, A.-G., & Buchner, A. (2007). G*Power 3: A flexible statistical power analysis program for the social, behavioral, and biomedical sciences. *Behavior Research Methods*, *39*, 175–191. https://doi.org/10.3758/BF03193146, PubMed: 17695343

Fetsch, C. R., Odean, N. N., Jeurissen, D., El-Shamayleh, Y., Horwitz, G. D., & Shadlen, M. N. (2018). Focal optogenetic suppression in macaque area MT biases direction discrimination and decision confidence, but only transiently. *eLife*, *7*, e36523. https://doi.org/10.7554/eLife.36523, PubMed: 30051817

Fries, P., & Maris, E. (2022). What to do if *N* is two? *Journal of Cognitive Neuroscience*, *34*, 1114–1118. https://doi.org/10.1162/jocn_a_01857, PubMed: 35468209

Ghosh, S., & Maunsell, J. H. R. (2024). Locus coeruleus norepinephrine contributes to visual–spatial attention by selectively enhancing perceptual sensitivity. *Neuron*, *112*, 2231–2240. https://doi.org/10.1016/j.neuron.2024.04.001, PubMed: 38701788

Herman, J. P., Arcizet, F., & Krauzlis, R. J. (2020). Attention-related modulation of caudate neurons depends on superior colliculus activity. *eLife*, *9*, e53998. https://doi.org/10.7554/eLife.53998, PubMed: 32940607

Herman, J. P., Katz, L. N., & Krauzlis, R. J. (2018). Midbrain activity can explain perceptual decisions during an attention task. *Nature Neuroscience*, *21*, 1651–1655. https://doi.org/10.1038/s41593-018-0271-5, PubMed: 30482945

Hikosaka, O., & Wurtz, R. H. (1985). Modification of saccadic eye movements by GABA-related substances. I. Effect of muscimol and bicuculline in monkey superior colliculus. *Journal of Neurophysiology*, *53*, 266–291. https://doi.org/10.1152/jn.1985.53.1.266, PubMed: 2983037

Hüer, J., Saxena, P., & Treue, S. (2024). Pathway-selective optogenetics reveals the functional anatomy of top–down attentional modulation in the macaque visual cortex. *Proceedings of the National Academy of Sciences, U.S.A.*, *121*, e2304511121. https://doi.org/10.1073/pnas.2304511121, PubMed: 38194453

Inoue, K.-I., Takada, M., & Matsumoto, M. (2015). Neuronal and behavioural modulations by pathway-selective optogenetic stimulation of the primate oculomotor system. *Nature Communications*, *6*, 8378. https://doi.org/10.1038/ncomms9378, PubMed: 26387804

Katz, L. N., Yates, J. L., Pillow, J. W., & Huk, A. C. (2016). Dissociated functional significance of decision-related activity in the primate dorsal stream. *Nature*, *535*, 285–288. https://doi.org/10.1038/nature18617, PubMed: 27376476

Katz, L. N., Yu, G., Herman, J. P., & Krauzlis, R. J. (2023). Correlated variability in primate superior colliculus depends on functional class. *Communications Biology*, *6*, 540. https://doi.org/10.1038/s42003-023-04912-0, PubMed: 37202508

Krauzlis, R. J., Lovejoy, L. P., & Zénon, A. (2013). Superior colliculus and visual spatial attention. *Annual Review of Neuroscience*, *36*, 165–182. https://doi.org/10.1146/annurev-neuro-062012-170249, PubMed: 23682659

Li, C. S., Mazzoni, P., & Andersen, R. A. (1999). Effect of reversible inactivation of macaque lateral intraparietal area on visual and memory saccades. *Journal of Neurophysiology*, *81*, 1827–1838. https://doi.org/10.1152/jn.1999.81.4.1827, PubMed: 10200217

Lovejoy, L. P., & Krauzlis, R. J. (2010). Inactivation of primate superior colliculus impairs covert selection of signals for perceptual judgments. *Nature Neuroscience*, *13*, 261–266. https://doi.org/10.1038/nn.2470, PubMed: 20023651

Martin, J. H. (1991). Autoradiographic estimation of the extent of reversible inactivation produced by microinjection of lidocaine and muscimol in the rat. *Neuroscience Letters*, *127*, 160–164. https://doi.org/10.1016/0304-3940(91)90784-Q, PubMed: 1881625

Nandy, A., Nassi, J. J., Jadi, M. P., & Reynolds, J. (2019). Optogenetically induced low-frequency correlations impair perception. *eLife*, *8*, e35123. https://doi.org/10.7554/eLife.35123, PubMed: 30794156

Ottes, F. P., Van Gisbergen, J. A., & Eggermont, J. J. (1986). Visuomotor fields of the superior colliculus: A quantitative model. *Vision Research*, *26*, 857–873. https://doi.org/10.1016/0042-6989(86)90144-6, PubMed: 3750869

Paxinos, G., Huang, X. F., Petrides, M., & Toga, A. (2008). *The rhesus monkey brain in stereotaxic coordinates*. Academic Press.

Robinson, D. A. (1972). Eye movements evoked by collicular stimulation in the alert monkey. *Vision Research*, *12*, 1795–1808. https://doi.org/10.1016/0042-6989(72)90070-3, PubMed: 4627952

Schneider, C. A., Rasband, W. S., & Eliceiri, K. W. (2012). NIH Image to ImageJ: 25 years of image analysis. *Nature Methods*, *9*, 671–675. https://doi.org/10.1038/nmeth.2089, PubMed: 22930834

Tremblay, S., Acker, L., Afraz, A., Albaugh, D. L., Amita, H., Andrei, A. R., et al. (2020). An open resource for non-human primate optogenetics. *Neuron*, *108*, 1075–1090. https://doi.org/10.1016/j.neuron.2020.09.027, PubMed: 33080229

Wang, L., McAlonan, K., Goldstein, S., Gerfen, C. R., & Krauzlis, R. J. (2020). A causal role for mouse superior colliculus in visual perceptual decision-making. *Journal of Neuroscience*, *40*, 3768–3782. https://doi.org/10.1523/JNEUROSCI.2642-19.2020, PubMed: 32253361

Wichmann, F. A., & Hill, N. J. (2001). The psychometric function: I. Fitting, sampling, and goodness of fit. *Perception & Psychophysics*, *63*, 1293–1313. https://doi.org/10.3758/BF03194544, PubMed: 11800458

Wilke, M., Kagan, I., & Andersen, R. A. (2012). Functional imaging reveals rapid reorganization of cortical activity after parietal inactivation in monkeys. *Proceedings of the National Academy of Sciences, U.S.A.*, *109*, 8274–8279. https://doi.org/10.1073/pnas.1204789109, PubMed: 22562793